Planning Model for Energy Routers Considering Peer-to-Peer Energy Transactions Among Multiple Distribution Networks

Meifu Chen, Mingchao Xia, *Senior Member*, *IEEE*, and Qifang Chen, *Member*, *IEEE*

***Abstract*—A high proportion of renewable energy affects the power quality of distribution networks, and surplus energy will be sold to the upstream grid at a low price. In this paper, considering peer-to-peer energy transactions, the energy router-based multiple distribution networks are analyzed to solve the above problems and realize collaborative consumption of renewable energy. Presently, the investing cost of an energy router is high, and research on the economic operation of energy routers in distribution networks is little. Therefore, this paper establishes a planning model for energy routers considering peer-to-peer energy transactions among distribution networks, and explores the benefits of peer-to-peer energy transactions through energy router based multiple distribution networks. A structure of an energy router suitable for peer-to-peer energy transactions is selected, and a power flow calculation model based on a multi-layer structure is established. The energy router's scheduling model is established, and unique functions of the energy router and revenue of each distribution network are considered. A power flow calculation model based on peer-to-peer interconnection of multiple distribution networks through energy routers is also established. Finally, simulation results verify the effectiveness of the proposed planning model. Results show that peer-to-peer energy transaction among distribution networks through energy routers can effectively reduce the comprehensive cost of distribution networks, significantly improve the power quality of the distribution networks, and reduce the impact of power fluctuation on the upstream grid incurred by the distribution network.**

***Index Terms*—Capacity allocation, energy router, multiple distribution networks, peer-to-peer energy transaction, power flow optimization.**

NOMENCLATURE

A. Abbreviations

ER	Energy router.
P2P, SDR	Peer-to-peer, supply and demand relationship.
DN, SST	Distribution network, solid-state transformer.
PET	Power electronic transformer.
DG	Distribution generation.
PV, WT	Photovoltaic, wind turbine.
AC, DC	Alternating current, direct current.
MISOCP	Mixed-integer second-order cone programming.
U-layer	User layer of the ER.
R-layer	Routing layer of the ER.
F-layer	Forwarding layer of the ER.

B. Parameters

$i \to j$	Bus i is the parent of bus j, and j is the child.
$L_{j,k}$, $Len_{j,k}$	Electric line from bus j and k, and its length.
$N_{\mathrm{ac}}^{\mathrm{bus},m}$	AC bus set in the original DN_m.
$N_{\mathrm{Uac}}^{\mathrm{ER},m}$	Port set of the U-layer in ER m.
$N_{\mathrm{Ulac}}^{\mathrm{ER},m}$	Port set of the new AC electric line closely to filter inductor branch of the U-layer in DN_m.
$N_{\mathrm{Rdc}}^{\mathrm{ER},m}$	Port set of the R-layer in ER m.
$N_{\mathrm{Fdc}}^{\mathrm{ER},m}$	Port set of the F-layer in ER m.
$C_{\mathrm{Uac}}^{\mathrm{U}}, C_{\mathrm{Rdc}}^{\mathrm{U}}$	Unit capacity cost of the U-layer and R-layer.
$C_{\mathrm{Fdc}}^{\mathrm{U}}$	Unit capacity cost of the F-layer.
$S_{\mathrm{ac}}^{\mathrm{ER}}, S_{\mathrm{dc}}^{\mathrm{ER}}$	Step capacity of the AC and DC converter port.
$d_{\mathrm{ac}}, y_{\mathrm{ac}}$	Discount rate and lifetime of the U-layer.
$\xi_{\mathrm{Uac}}, \xi_{\mathrm{Rac}}$	Unit operation cost of the U-layer and R-layer.
ξ_{Fac}	Unit operation cost of the F-layer.
$C_{\mathrm{pac}}^{\mathrm{line}}, C_{\mathrm{pdc}}^{\mathrm{line}}$	Unit investing cost of a single AC and DC line.
$\tau_{\mathrm{ac}}, \varphi_{\mathrm{ac}}$	Discount rate and lifetime of AC electric line.
$\tau_{\mathrm{dc}}, \varphi_{\mathrm{dc}}$	Discount rate and lifetime of DC electric line.
λ_{P}	Penalty price of the energy loss.
T_{h}	Operation hours of load and source.
r_{ij}, x_{ij}	Resistance and reactance of branch $\mathrm{L}_{i,j}$.
$r_{jk}^{\mathrm{er},m}, x_{jk}^{\mathrm{er},m}$	Resistance and reactance of equivalent inductor branch $\mathrm{L}_{j,k}$ of the port at U-layer in ER_m.
$r_{ij}^{\mathrm{L},m}, x_{ij}^{\mathrm{L},m}$	Resistance and reactance of new electric line $\mathrm{L}_{i,j}$ built for the U-layer in ER_m.
$\mathrm{M}_1 \sim \mathrm{M}_5$	Positive big numbers for constraints.
$N_{\mathrm{Uac}}^{\max}, N_{\mathrm{Rdc}}^{\max}$	Maximal step values of the U-layer and R-layer.
N^{DN}, N_s	Number of DNs and time slots.
N_{bus}^m	Number of buses in DN_m
$a_1 \sim a_3$	Parameters of the SDR-based clearing price.

C. Variables

m	The index of the DN and the ER.
$C_{\mathrm{Uac}}^{\mathrm{ER},m}, C_{\mathrm{Rdc}}^{\mathrm{ER},m}$	Capacity cost of the U-layer and R-layer.

Manuscript received July 21, 2021; revised November 9, 2021; accepted February 7, 2022. Date of online publication October 12, 2022; date of current version March 31, 2023. This work was supported in part by the Fundamental Research Funds for the Central Universities under Grant 2018JBZ004.

M. F. Chen, M. C. Xia (corresponding author, email: mchxia@bjtu.edu.cn; ORCID: https://orcid.org/0000-0003-2110-5699), and Q. F. Chen are with School of Electrical Engineering, Beijing Jiaotong University, Beijing 100044, China.

DOI: 10.17775/CSEEJPES.2021.05270

$C_{\mathrm{ac}}^{\mathrm{line},m}, C_{\mathrm{dc}}^{\mathrm{line},m}$	Investing cost of the new AC and DC electric lines for connecting ER_m.
C_{om}	Operation and maintenance cost of ER_m.
C_{loss}	Energy loss cost of the ER-based DN_m.
$\pi_{\mathrm{Uac},j}^{\mathrm{ER},m}, \pi_{\mathrm{Rdc},j}^{\mathrm{ER},m}, \pi_{\mathrm{Fdc},j}^{\mathrm{ER},m}$	Positive integer variables configuring capacity of the port j at the U-layer, R-layer and F-layer in ER_m, respectively.
$\delta_{\mathrm{Uac},j}^{\mathrm{ER},m}, \delta_{\mathrm{dc},j}^{\mathrm{ER},m}$	Binary variables configuring AC and DC lines.
$\delta_{\mathrm{Rdcp},s}^{\mathrm{ER},m}$	Binary variable indicating the power direction of the R-layer.
$\delta_{\mathrm{up},s}^{m}, \delta_{\mathrm{Rup},j,s}^{\mathrm{ER},m}$	Auxiliary binary variables calculating the cost.
$s, \Delta T$	Scenario variable, and time step of scenario s.
$I_{ij,s}, U_{i,s}$	Branch current from bus i to j, voltage of bus i.
$\hat{I}_{ij,s}, \hat{U}_{i,s}$	Denote $I_{ij,s}^2$ and $U_{i,s}^2$, respectively.
$P_{jk,s}, Q_{jk,s}$	Branch active and reactive power output from bus j, and the electric line loss of L_{jk} is not included. The direction is from j to k.
$P_{ig,s}, Q_{ig,s}$	Active and reactive power of the source at bus j.
$P_{dj,s}, Q_{dj,s}$	Active and reactive power of the load at bus j.
$P_{\mathrm{Uac},i,s}^{\mathrm{ER},m}, Q_{\mathrm{Uac},i,s}^{\mathrm{ER},m}$	Active and reactive port power of the U-layer.
$P_{\mathrm{Rdc},i,s}^{\mathrm{ER},m}, P_{\mathrm{Fdc},i,s}^{\mathrm{ER},m}$	Port Power at the R-layer and F-layer.
$S_{\mathrm{Uac},i}^{\mathrm{ER},m}, S_{\mathrm{Rdc},i}^{\mathrm{ER},m}$	Capacity of ports at the U-layer and R-layer.
$S_{\mathrm{Fdc},i}^{\mathrm{ER},m}$	Capacity of port i at the F-layer.
$P_{\mathrm{Rdc},j,s}^{\mathrm{ERin},m}, P_{\mathrm{Rdc},j,s}^{\mathrm{ERout},m}$	Auxiliary positive variables of $P_{\mathrm{Rdc},i,s}^{\mathrm{ER},m}$.
$P_{\mathrm{up},s}^{\mathrm{in},m}, P_{\mathrm{up},s}^{\mathrm{out,\,m}}$	Auxiliary positive variables of $P_{ig,s}$ at slack bus.
$C_{\mathrm{p2p},s}^{\mathrm{buy}}, C_{\mathrm{p2p},s}^{\mathrm{sell}}$	Purchasing and selling prices of the P2P market.
$C_{\mathrm{up},s}^{\mathrm{buy}}, C_{\mathrm{up},s}^{\mathrm{sell}}$	Purchasing and selling prices of upstream grid.
f_{sys}, f_m	Total cost of the entire system, cost of DN_m.
$K_{\mathrm{var\_}m}$	Index of exchanging power volatility of DN_m.
$K_{\mathrm{vol\_}m}$	Voltage deviation index of DN_m.
$K_{\mathrm{gap\_}m}$, K_{gapdc}	Relaxing gap of DN_m and the DC system.

I. Introduction

A high proportion of distributed generation (DG) installed in a distribution network (DN) usually causes bus voltage violation and bidirectional power flow [1], [2]. Besides, because of the randomness and volatility of DG and load, energy shortage or surplus energy occurs within the DN. Thus, a DN with energy shortage needs to purchase energy from the upstream grid at a high price, and that with energy surplus will sell the surplus energy at a low price [3], [4]. Such a process will reduce the benefits of installing DG. As the power of load and DG within a DN in different regions vary enormously, peer-to-peer (P2P) energy transactions are adopted to solve the above issues in this paper. Then, energy fluctuation within DNs can be first alleviated among different DNs with the same rated voltage, and revenue of DG can also be gained, and the adverse impact of power fluctuations on the upstream grid will also be reduced [5]–[7]. However, both the consumption of DG within the DN and P2P energy transactions among different DNs require the DN should have efficient and fast network control methods [8], [9].

Recently, an energy router (ER) aims to solve issues such as bi-directional power flow, voltage matching and energy matching incurred by DG [10]. Such a device is a multi-port converter with flexible energy flow controllability to facilitate access and energy management of different devices. Typical topology of an ER is based on a solid-state transformer (SST) with three stages, so it is also called a power electronic transformer (PET) [11], [12]. Presently, research on the ER mainly focuses on its structure design, and transient control strategy [13]–[15]. As a multi-port device with flexible energy management, a P2P energy transaction is also a vital application of the ER, and its application in a DC network has been studied. In [7], the ER acts as an agent, and a P2P energy matching mechanism is proposed to carry out the power transaction price, transaction pair and power transmission path. In [16], a distributed P2P energy sharing strategy is proposed to obtain the transmission path with minimum power loss. The ER is regarded as the aggregator of electric energy in the microgrid, dynamically changing the role between load and source according to its energy balance. In [17], [18], a distributed method for calculating the minimum loss path of power transmission is proposed to promote P2P energy transactions between source and load. This paper mainly focuses on power flow optimization in ER-based DN, and studies an optimal configuration scheme of multiple ERs considering P2P energy transactions among multiple DNs.

Much research analyzes power flow optimization in the ER-based electric grid. The power flow calculation model of an ER with an isolation stage is established in [19], and an ER is applied in the transmission network to replace a branch transformer. Power regulation of the weak branch is achieved in the network. In [20], the ER is deployed to realize interconnection of the alternating current (AC) and direct current (DC) transmission network and the integration of DG. Device-level control strategy is considered in the power flow calculation model. In [21], the ER is applied to the DN. Replacing the critical bus with the ER and connecting some vital buses through the ER are conducted, respectively. Results show that it can improve power quality of the DN. In [22], the ER internally integrated with a DC microgrid is connected with multiple buses of the DN. Power flow optimization of the ER-based DN is carried out to minimize fuel cost of generators and network loss. An optimization model is divided to solve in a distributed way. In [23], the power flow calculation model of the DN with multiple ERs is established, and a faster iterative method to solve the power

flow calculation is proposed. In [24], considering the influence of an integrated energy system on optimal operation of the DN, the ER is used as a grid-connecting interface. Multiple ERs share energy through medium-voltage DC electric lines, and power flow optimization of the DN is also achieved. In [25], a semi-definite programming-based power flow optimization model of an ER-based DN is developed to solve it efficiently. In [26], interconnection of the AC and DC microgrid system is realized by multiple ERs, and power flow optimization and energy sharing between different systems are realized. In sum, the above research shows the ER can alleviate issues such as voltage violation and network loss. However, the above research considers little about economic operation of an ER, and P2P energy transactions among DNs based on ERs needs to be analyzed.

There are few studies about planning of the ER, and mainly for planning of PET acting as a grid-connecting interface. The optimal configuration of ER in DN, considering P2P energy transactions, has not been found yet. In [27], the optimal configuration of PET from the perspective of DN is analyzed, and reactive power regulation capacities of medium-voltage AC port and low-voltage AC port are fully exploited to optimize network loss of DN. However, such an application does not utilize the active power controllability of ER. The economic configuration is also not considered. In [28], the capacity configurations of PET, photovoltaic (PV), wind turbine (WT), energy storage and other equipment in the microgrid are analyzed, and the PET acts as an interface. The output of each device and real-time electricity price are considered, but power flow of the DN is not involved. Thus, such a method is difficult to apply to the DN.

The soft open point (SOP) has a similar function but is mainly viewed as a substitution for a tie-switch to optimize power flow of interconnected feeders, which differs from the function of ER [29], [30]. In this paper, an energy router is designed to optimize operation of the distribution network and to achieve peer-to-peer energy trading. Location of the energy router is according to its requirements. Thus, functions of the energy router and SOP are different. When each distribution network configures only one energy router to work alone, the functions of the energy router and SOP are similar if the energy router is not equipped with renewable energy. Such a situation will be simulated in case A2 of Section IV.

Therefore, this paper will study the planning of multiple ERs considering P2P energy transactions among different DNs. Impact incurred by the ER on power quality and economical operation of the DN will be the main focus. Optimal configurations of ERs will also be obtained. In [31], a multi-layer structure-based ER is designed to manage power flow of the DN, and route energy between ERs, and forward energy for other ERs. Thus, such a structure may be more suitable for P2P energy transactions, and adopted in this paper.

In [32], [33], energy balance within the peer-to-peer energy sharing system and trading price are targets, and a typical optimization model is usually built to solve the problem. Such studies have less consideration for the different requirements of power quality between source and load. In [16]–[18], an energy transmission path between source and load is the focus, and the shortest path algorithm such as Dijkstra is usually deployed to solve such a problem. Considering the price should be low if power quality of the source is poor, different requirements of power quality between source and load can be easily met. In this paper, for simplicity, power quality of the source is ignored. The planning model of energy routers belongs to an optimization problem, and thus it is more appropriate to adopt the method shown in [32], [33] rather than that in [16]–[18].

The configuration includes capacity of ports in the user-layer, routing-layer and forwarding-layer of ERs. Configuration of new electric lines for connecting the ER is also considered. Finally, the proposed planning model is transformed into a mixed-integer second-order cone programming (MISOCP) model to solve effectively [29]. The main contributions are as follows:

1) The benefit of ERs-based multiple DNs with P2P energy transactions is explored, which analyzes the economic value for research on P2P energy transactions among ER-based DNs;

2) A planning model of multiple ERs considering P2P energy transactions among DNs is established to obtain the optimal configuration scheme of ERs. Such a scheme optimizes power quality of DNs, collaboratively consumes power fluctuations of DNs at the same rated voltage side, and alleviates adverse impacts on the upstream grid;

3) A dispatching model of ER is proposed considering transactions of electric energy in DN, considering the unique structure and function of the ER and revenue of the DN. A power flow calculation model considering P2P interconnection of DNs through ERs is established;

4) Considering the ER includes user-layer, routing-layer and forwarding-layer, the multi-layer structure based power flow calculation model of an ER is established to facilitate P2P energy transactions.

Section II presents ERs-based interconnecting DNs. A planning model is presented in Section III. Section IV specifies simulation cases and results analysis. Finally, conclusions are summarized in Section V.

II. ERs-based interconnecting DNs

A. ERs-based P2P Energy Sharing Structure Among DNs

Based on an ERs system, a P2P energy sharing structure of multiple DNs is shown in Fig. 1. First, each ER connects with a DN through multiple buses to facilitate power flow optimization of the DN and maximize consumption of DG. Second, P2P interconnecting electric lines between the ERs are built individually. Energy sharing between interconnecting ERs is controlled through high-speed communication to facilitate P2P energy transactions. Meanwhile, a P2P trader should be constructed to coordinate P2P energy transactions among DNs, and communicate with the ERs for information exchange in a low-speed way.

A P2P transaction structure is shown in Fig. 1, and the ER has three main functions: a) optimizing power flow of the DN; b) selling surplus power to other ERs or purchasing energy from other ERs [7]; c) forwarding energy from one path to the target if the ER is in the energy transmission path of a P2P trading pair formed by others.

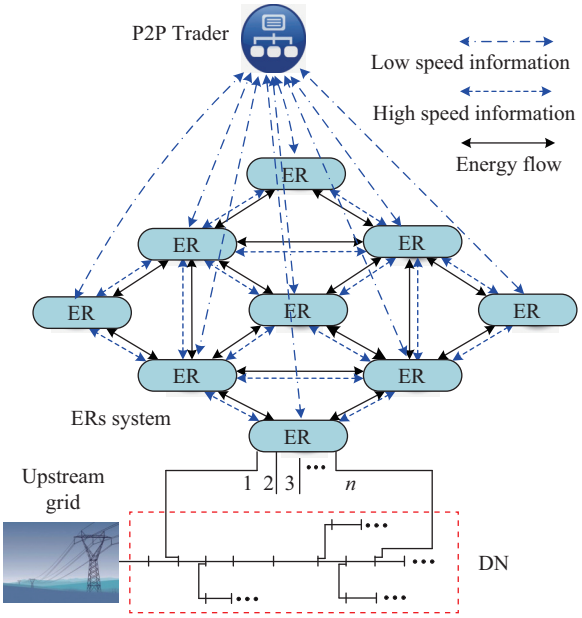

Fig. 1. Energy sharing structure among the ERs-based DNs.

B. Power Flow Calculation Model of the ER Applicable for P2P Energy Transactions

In [31], the structure of multi-layer-based ER mainly includes user-layer (U-layer), routing-layer (R-layer) and forwarding-layer (F-layer), and is adopted in this paper. A simplified structure is shown in Fig. 2. The U-layer connects with the DN for optimizing power flow and improving power quality of the DN. R-layer is in charge of P2P energy transactions between different DNs. Surplus power of the DN is sold to other DNs through R-layer, and energy support is also met through the R-layer.

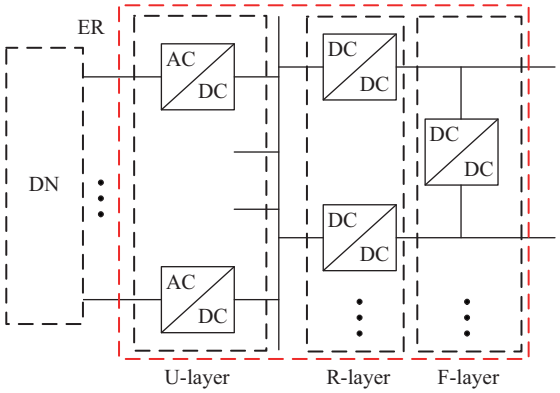

Fig. 2. The ER structure applicable for P2P energy transactions.

F-layer is placed between ports of the R-layer, and thus it can forward energy for R-layer or other ERs. Generally, the capacity of electric lines is larger than ports of ER. When expected output energy of one port at R-layer is larger than its rated capacity, some of the energy can be output by other ports at R-layer and forwarded to corresponding electric lines by ports at F-layer. When the ER is in the routing path of energy transactions between other DNs, F-layer rather than R-layer forwards the energy directly from an electric line to the target. Such a design of the ER makes functions of each layer work independently, and facilitates P2P energy transactions.

According to the ER model established in [19], [22], converter loss is replaced by an equivalent resistor. Thus, an equivalent model of the ER, adopted in this paper, is shown in Fig. 3, and a proposed power flow calculation model is shown below.

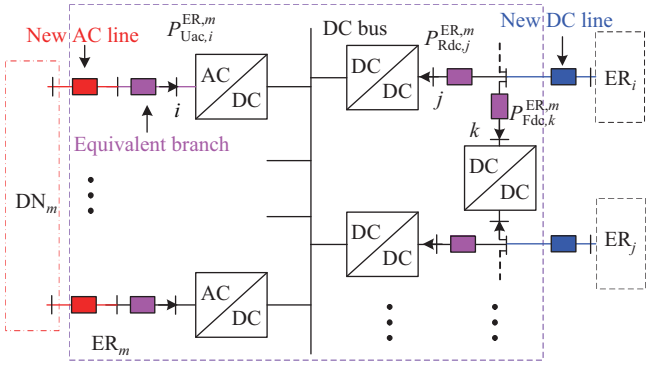

Fig. 3. Model of the ER applicable for P2P energy transactions.

1) Energy Balance of the DC Bus Inside the ER

Energy balance of the DC bus is kept by U-layer and R-layer and is shown in (1).

$$\sum_i P^{\mathrm{ER},m}_{\mathrm{Uac},i,s} + \sum_j P^{\mathrm{ER},m}_{\mathrm{Rdc},j,s} = 0,\ i \in N^{\mathrm{ER},m}_{\mathrm{Uac}},\ j \in N^{\mathrm{ER},m}_{\mathrm{Rdc}} \tag{1}$$

2) Modeling Ports at U-layer

Each port of U-layer consists of an AC/DC converter, and its equivalent impedance branch includes a filter inductor and equivalent resistor. (2) and (3) represent the energy balance of a port of U-layer, and (4) calculates branch power from the connecting point of a new AC electric line. (5) restricts voltages between both ends of the equivalent impedance branch of the port of U-layer. (6) denotes the capacity constraint of the port of the U-layer.

$$\sum_{j:j\to k}(P_{jk,s} - r^{\mathrm{er},m}_{jk} I^2_{jk,s}) = P^{\mathrm{ER},m}_{\mathrm{Uac},k,s},\quad j \in N^{\mathrm{ER},m}_{\mathrm{Ulac}},\ k \in N^{\mathrm{ER},m}_{\mathrm{Uac}} \tag{2}$$

$$\sum_{j:j\to k}(Q_{jk,s} - x^{\mathrm{er},m}_{jk} I^2_{jk,s}) = Q^{\mathrm{ER},m}_{\mathrm{Uac},k,s},\quad j \in N^{\mathrm{ER},m}_{\mathrm{Ulac}},\ k \in N^{\mathrm{ER},m}_{\mathrm{Uac}} \tag{3}$$

$$U^2_{i,s} I^2_{ij,s} = P^2_{ij,s} + Q^2_{ij,s},\ i \to j,\ i \in N^{\mathrm{ER},m}_{\mathrm{Ulac}},\ j \in N^{\mathrm{ER},m}_{\mathrm{Uac}} \tag{4}$$

$$U^2_{j,s} = U^2_{i,s} - 2(r^{\mathrm{er},m}_{ij} P_{ij,s} + x^{\mathrm{er},m}_{ij} Q_{ij,s}) + I^2_{ij,s}\left[(r^{\mathrm{er},m}_{ij})^2 + (x^{\mathrm{er},m}_{ij})^2\right],\ i \to j,\ i \in N^{\mathrm{ER},m}_{\mathrm{Ulac}},\ j \in N^{\mathrm{ER},m}_{\mathrm{Uac}} \tag{5}$$

$$(P^{\mathrm{ER},m}_{\mathrm{Uac},i,s})^2 + (Q^{\mathrm{ER},m}_{\mathrm{Uac},i,s})^2 \le (S^{\mathrm{ER},m}_{\mathrm{Uac},i})^2,\ i \in N^{\mathrm{ER},m}_{\mathrm{Uac}} \tag{6}$$

New electric lines should be built for electrical connections when ports of U-layer are far from their connecting buses in the DN. Branches of such new electric lines are added to U-layer to develop a general model of an ER. (7) and (8) denote

the energy balance of the end of the new line connected with U-layer. (9) denotes branch power from the other terminal of the new line connected with the bus of the DN. (10) restricts voltages between both ends of the new line, and (11) denotes the capacity constraint of the new line.

$$\sum_{i:i\to j}(P_{ij,s}-r_{ij}^{\mathrm{L},m}I_{ij,s}^2)=\sum_{j:j\to k}P_{jk,s},\quad j\in N_{\mathrm{Ulac}}^{\mathrm{ER},m},\ k\in N_{\mathrm{Uac}}^{\mathrm{ER},m} \tag{7}$$

$$\sum_{i:i\to j}(Q_{ij,s}-x_{ij}^{\mathrm{L},m}I_{ij,s}^2)=\sum_{j:j\to k}Q_{jk,s},\quad j\in N_{\mathrm{Ulac}}^{\mathrm{ER},m},\ k\in N_{\mathrm{Uac}}^{\mathrm{ER},m} \tag{8}$$

$$U_{i,s}^2I_{ij,s}^2=P_{ij,s}^2+Q_{ij,s}^2,\ i\to j,\ i\in N_{\mathrm{ac}}^{\mathrm{bus},m},\ j\in N_{\mathrm{Ulac}}^{\mathrm{ER},m} \tag{9}$$

$$U_{j,s}^2=U_{i,s}^2-2(r_{ij}^{\mathrm{L},m}P_{ij,s}+x_{ij}^{\mathrm{L},m}Q_{ij,s})+I_{ij,s}^2\left[(r_{ij}^{\mathrm{L},m})^2+(x_{ij}^{\mathrm{L},m})^2\right],\ i\to j,\ i\in N_{\mathrm{ac}}^{\mathrm{bus},m},\ j\in N_{\mathrm{Ulac}}^{\mathrm{ER},m} \tag{10}$$

$$(P_{ij,s})^2+(Q_{ij,s})^2\le(S_{ij}^{\mathrm{N}})^2,\ i\in N_{\mathrm{ac}}^{\mathrm{bus},m},\ j\in N_{\mathrm{Ulac}}^{\mathrm{ER},m} \tag{11}$$

3) Modeling of Ports at R-layer

Power flow of R-layer is more complex than those of the U-layer because of the P2P electrical connection. The port of R-layer can be either a parent bus or a child bus. Therefore, it is not easy to individually list the power flow relationship of R-layer similar to U-layer. Only the capacity constraint (12) is given. The power flow relationship of R-layer will be listed in the P2P transaction part.

$$-S_{\mathrm{Rdc},j}^{\mathrm{ER},m}\le P_{\mathrm{Rdc},j,s}^{\mathrm{ER},m}\le S_{\mathrm{Rdc},j}^{\mathrm{ER},m},\ j\in N_{\mathrm{Rdc}}^{\mathrm{ER},m} \tag{12}$$

4) Modeling of Ports at F-layer

In Fig. 3, each converter of F-layer has two ends, and energy balance and capacity limit are shown in (13) and (14), respectively. An equivalent resistor of the converter is placed at one side of the converter.

$$\sum_k P_{\mathrm{Fdc},k,s}^{\mathrm{ER},m}=0,\ k\in N_{\mathrm{Fdc},i}^{\mathrm{ER},m} \tag{13}$$

$$-S_{\mathrm{Fdc},i}^{\mathrm{ER},m}\le P_{\mathrm{Fdc},k,s}^{\mathrm{ER},m}\le S_{\mathrm{Fdc},i}^{\mathrm{ER},m},\ k\in N_{\mathrm{Fdc},i}^{\mathrm{ER},m},\ i\in N_{\mathrm{Fdc}}^{\mathrm{ER},m} \tag{14}$$

III. Planning Model of ERs Considering P2P Energy Transactions among DNs

A. Comprehensive Annual Cost of a Single ER-based DN

Comprehensive annual cost (f_m) of an ER-based DN_m includes: a) capacity investing cost of ports at U-layer, R-layer and F-layer; b) investing cost of new AC electric lines for U-layer; c) investing cost of new DC electric lines for R-layer; d) operation and maintenance cost of the ER; e) network loss cost of the DN; f) energy transaction cost with the upstream grid; g) energy transaction cost in the P2P market with other DNs. f_m is shown in (15). Note the energy forwarding cost of F-layer is not considered in this paper.

$$f_m=C_{\mathrm{Uac}}^{\mathrm{ER},m}+C_{\mathrm{Rdc}}^{\mathrm{ER},m}+C_{\mathrm{Fdc}}^{\mathrm{ER},m}+C_{\mathrm{ac}}^{\mathrm{line},m}+C_{\mathrm{dc}}^{\mathrm{line},m}+C_{\mathrm{om}}^{m}+C_{\mathrm{loss}}^{m}+C_{\mathrm{trade}}^{m}+C_{\mathrm{p2p}}^{m} \tag{15}$$

1) Capacity investing cost of ports at U-layer

$$\begin{cases}C_{\mathrm{Uac}}^{\mathrm{ER},m}=C_{\mathrm{Uac}}^{\mathrm{U}}\frac{d_{\mathrm{ac}}(1+d_{\mathrm{ac}})^{y_{\mathrm{ac}}}}{(1+d_{\mathrm{ac}})^{y_{\mathrm{ac}}}-1}\sum_{j\in N_{\mathrm{Uac}}^{\mathrm{ER},m}}S_{\mathrm{Uac},j}^{\mathrm{ER},m}\\ S_{\mathrm{Uac},j}^{\mathrm{ER},m}=\pi_{\mathrm{Uac},j}^{\mathrm{ER},m}S_{\mathrm{ac}}^{\mathrm{ER}}\end{cases} \tag{16}$$

2) Capacity investing cost of ports at R-layer

$$\begin{cases}C_{\mathrm{Rdc}}^{\mathrm{ER},m}=C_{\mathrm{Rdc}}^{\mathrm{U}}\frac{d_{\mathrm{dc1}}(1+d_{\mathrm{dc1}})^{y_{\mathrm{dc1}}}}{(1+d_{\mathrm{dc1}})^{y_{\mathrm{dc1}}}-1}\sum_{j\in N_{\mathrm{Rdc}}^{\mathrm{ER},m}}S_{\mathrm{Rdc},j}^{\mathrm{ER},m}\\ S_{\mathrm{Rdc},j}^{\mathrm{ER},m}=\pi_{\mathrm{Rdc},j}^{\mathrm{ER},m}S_{\mathrm{dc}}^{\mathrm{ER}}\end{cases} \tag{17}$$

3) Capacity investing cost of ports at F-layer

The converter of F-layer consists of two ends, but they belong to the same converter. Thus, (18) denotes that capacities of both ends are the same. To derive a general model, investing cost shown in (19) is divided into two parts.

$$\begin{cases}S_{\mathrm{Fdc},j}^{\mathrm{ER},m}=\pi_{\mathrm{Fdc},j}^{\mathrm{ER},m}S_{\mathrm{dc}}^{\mathrm{ER}}\\ S_{\mathrm{Fdc},j}^{\mathrm{ER},m}=S_{\mathrm{Fdc},k}^{\mathrm{ER},m},\ j,k\in N_{\mathrm{Fdc},i}^{\mathrm{ER},m},\ i\in N_{\mathrm{Fdc}}^{\mathrm{ER},m}\end{cases} \tag{18}$$

$$C_{\mathrm{Fdc}}^{\mathrm{ER},m}=0.5C_{\mathrm{Fdc}}^{\mathrm{U}}\frac{d_{\mathrm{dc2}}(1+d_{\mathrm{dc2}})^{y_{\mathrm{dc2}}}}{(1+d_{\mathrm{dc2}})^{y_{\mathrm{dc2}}}-1}\sum_{j\in N_{\mathrm{Fdc},i}^{\mathrm{ER},m}}S_{\mathrm{Fdc},j}^{\mathrm{ER},m} \tag{19}$$

4) Investing cost of new AC electric lines for U-layer

A new AC electric line consists of three lines denoting three-phase, and a coefficient of three is multiplied in (20).

$$C_{\mathrm{ac}}^{\mathrm{line},m}=\frac{3C_{\mathrm{pac}}^{\mathrm{line}}\tau_{\mathrm{ac}}(1+\tau_{\mathrm{ac}})^{\varphi_{\mathrm{ac}}}}{(1+\tau_{\mathrm{ac}})^{\varphi_{\mathrm{ac}}}-1}\sum_{i\to j}\delta_{\mathrm{Uac},j}^{\mathrm{ER},m}L_{i,j},\ j\in N_{\mathrm{Ulac}}^{\mathrm{ER},m} \tag{20}$$

5) Investing cost of new DC electric lines for R-layer

$$C_{\mathrm{dc}}^{\mathrm{line},m}=\begin{cases}C_{\mathrm{pdc}}^{\mathrm{line}}\frac{\tau_{\mathrm{dc}}(1+\tau_{\mathrm{dc}})^{\varphi_{\mathrm{dc}}}}{(1+\tau_{\mathrm{dc}})^{\varphi_{\mathrm{dc}}}-1}\sum_{i\to j}\delta_{\mathrm{dc},i}^{\mathrm{ER},m}Len_{i,j}, & \text{if } i\in N_{\mathrm{ldc}}^{\mathrm{ER},m}\\ C_{\mathrm{pdc}}^{\mathrm{line}}\frac{\tau_{\mathrm{dc}}(1+\tau_{\mathrm{dc}})^{\varphi_{\mathrm{dc}}}}{(1+\tau_{\mathrm{dc}})^{\varphi_{\mathrm{dc}}}-1}\sum_{i\to j}\delta_{\mathrm{dc},i}^{\mathrm{ER},m}Len_{i,j}, & \text{if } j\in N_{\mathrm{ldc}}^{\mathrm{ER},m}\end{cases} \tag{21}$$

Interconnected DNs shall bear half the investing cost of new DC electric lines for their own R-layer. The port of the U-layer can be the parent bus or the child bus, and the relationship is shown in (21).

6) Operation and maintenance cost of the ER

Operation and maintenance cost listed in (22) of the ER consists of the cost at U-layer, R-layer and F-layer.

$$C_{\mathrm{om}}^{m}=\xi_{\mathrm{Uac}}\sum_{j\in N_{\mathrm{Uac}}^{\mathrm{ER},m}}S_{\mathrm{Uac},j}^{\mathrm{ER},m}+\xi_{\mathrm{Rdc}}\sum_{j\in N_{\mathrm{Rdc}}^{\mathrm{ER},m}}S_{\mathrm{Rdc},j}^{\mathrm{ER},m}+0.5\xi_{\mathrm{Fdc}}\sum_{j\in N_{\mathrm{Fdc},i}^{\mathrm{ER},m}}S_{\mathrm{Fdc},j}^{\mathrm{ER},m} \tag{22}$$

7) Energy Loss Cost of the DN

Energy loss costs listed in (23)–(29) include loss of DN_m, new AC electric lines, new DC electric lines, and U-layer, R-layer and F-layer of ER_m. Considerable network loss will accelerate ageing of the above devices, and thus a penalty should be imposed. (26) indicates that energy loss of the DC lines is half shared by the interconnected ERs.

$$C_{\mathrm{loss}}^{m}=\lambda_{\mathrm{P}}T_{\mathrm{h}}\Delta T(P_{\mathrm{netloss}}^{m}+P_{\mathrm{acloss}}^{m}+P_{\mathrm{dcloss}}^{m}+P_{\mathrm{Uloss}}^{\mathrm{ER},m}+P_{\mathrm{Rloss}}^{\mathrm{ER},m}+P_{\mathrm{Floss}}^{\mathrm{ER},m}) \tag{23}$$

$$P^{m}_{\text{netloss}} = \sum_{s,i\to j} r_{ij} I^2_{ij,s},\ i,j \in N^{\text{bus},m}_{\text{ac}} \tag{24}$$

$$P^{m}_{\text{acloss}} = \sum_{s,i\to j} r^{\text{L}}_{ij} I^2_{ij,s},\ i \in N^{\text{bus},m}_{\text{ac}},\ j \in N^{\text{ER},m}_{\text{Ulac}} \tag{25}$$

$$P^{m}_{\text{dcloss}} = \begin{cases} \frac{1}{2}\sum_{s,\ i\in N^{\text{ER},m}_{\text{ldc}}} r_{ij} I^2_{ij,s}, & \text{if } i \to j \\ \frac{1}{2}\sum_{s,\ i\in N^{\text{ER},m}_{\text{ldc}}} r_{ij} I^2_{ji,s}, & \text{else} \end{cases} \tag{26}$$

$$P^{\text{ER},m}_{\text{Uloss}} = \sum_{s,i\to j} r^{\text{er}}_{jk} I^2_{ij,s},\ i \in N^{\text{ER},m}_{\text{Ulac}},\ j \in N^{\text{ER},m}_{\text{Uac}} \tag{27}$$

$$P^{\text{ER},m}_{\text{Rloss}} = \begin{cases} \sum_{s,i\to j} r_{ij} I^2_{ij,s}, & \text{if } i \in N^{\text{ER},m}_{\text{Rdc}} \\ \sum_{s,i\to j} r_{ij} I^2_{ij,s}, & \text{if } j \in N^{\text{ER},m}_{\text{Rdc}} \end{cases} \tag{28}$$

$$P^{\text{ER},m}_{\text{Floss}} = \sum_{s,i\to j} r_{ij} I^2_{ij,s},\ i \in N^{\text{ER},m}_{\text{Rldc}},\ j \in N^{\text{ER},m}_{\text{Fdc}} \tag{29}$$

8) Energy transaction cost with the upstream grid

Exchanging power between DN_m and upstream grid is split into two parts in (31) to calculate the energy cost in (30).

$$C^{m}_{\text{trade}} = T_{\text{h}} \Delta T \sum_{s} \left(C^{\text{buy}}_{\text{up},s} P^{\text{in},m}_{\text{up},s} - C^{\text{sell}}_{\text{up},s} P^{\text{out},m}_{\text{up},s} \right) \tag{30}$$

$$P_{ig,s} = P^{\text{in},m}_{\text{up},s} - P^{\text{out},m}_{\text{up},s},\ i \in N^{\text{slack},m}_{\text{ac}} \tag{31}$$

The splitting process in (32) is by adding binary variables. Then, the cost calculating model between DN_m and the upstream grid becomes linear. Such a conversion is a typical way to tackle a problem with bidirectional power. If no binary variable is added, a cost calculating model between DN_m and the upstream grid should be a piecewise nonlinear function of $P_{ig,s}$.

$$\begin{cases} 0 \le P^{\text{in},m}_{\text{up},s} \le P^{\text{in},m}_{\text{up,max}} (1 - \delta^{m}_{\text{up},s}) \\ 0 \le P^{\text{out},m}_{\text{up},s} \le P^{\text{out},m}_{\text{up,max}} \delta^{m}_{\text{up},s} \end{cases} \tag{32}$$

9) Energy transaction cost with other DNs

Cost calculation of the P2P energy transactions is similar, and is shown in (33)–(35).

$$C^{m}_{\text{p2p}} = T_{\text{h}} \Delta T \sum_{j,s} \left(C^{\text{buy},m}_{\text{p2p},s} P^{\text{ERin},m}_{\text{Rdc},j,s} - C^{\text{sell},m}_{\text{p2p},s} P^{\text{ERout},m}_{\text{Rdc},j,s} \right),\ j \in N^{\text{ER},m}_{\text{Rdc}} \tag{33}$$

$$P^{\text{ER},m}_{\text{Rdc},j,s} = P^{\text{ERin},m}_{\text{Rdc},j,s} - P^{\text{ERout},m}_{\text{Rdc},j,s},\ j \in N^{\text{ER},m}_{\text{Rdc}} \tag{34}$$

$$\begin{cases} 0 \le P^{\text{ERin},m}_{\text{Rdc},j,s} \le P^{\text{in},m}_{\text{Rup,max}} (1 - \delta^{\text{ER},m}_{\text{Rup},j,s}), & j \in N^{\text{ER},m}_{\text{Rdc}} \\ 0 \le P^{\text{ERout},m}_{\text{Rdc},j,s} \le P^{\text{out},m}_{\text{Rup,max}} \delta^{\text{ER},m}_{\text{Rup},j,s}, & j \in N^{\text{ER},m}_{\text{Rdc}} \end{cases} \tag{35}$$

B. Configuration and Operation Constraints of the ER

1) Constraints of U-layer and its new AC lines

Each port of U-layer and its corresponding new AC electric line are deployed together by constraints (36)–(37).

$$\pi^{\text{ER},m}_{\text{Uac},j} \le N^{\max}_{\text{Uac}} \delta^{\text{ER},m}_{\text{Uac},i},\ i \to j,\ i \in N^{\text{ER},m}_{\text{Ulac}},\ j \in N^{\text{ER},m}_{\text{Uac}} \tag{36}$$

$$\delta^{\text{ER},m}_{\text{Uac,i}} \le \pi^{\text{ER},m}_{\text{Uac,j}},\ i \to j,\ i \in N^{\text{ER},m}_{\text{Ulac}},\ j \in N^{\text{ER},m}_{\text{Uac}} \tag{37}$$

Besides, only when the new AC electric lines and ports of U-layer are configured, can branch currents be allowed.

$$\sum_{i:i\to k} I^2_{\text{ik,s}} \le M_1 \delta^{\text{ER},m}_{\text{Uac},l},\ i \in N^{\text{bus}}_{\text{ac}},\ k \in N^{\text{ER},m}_{\text{Ulac}} \tag{38}$$

$$\sum_{i:i\to j} I^2_{ij,s} \le M_2 \pi^{\text{ER},m}_{\text{Uac},j},\ i \in N^{\text{ER},m}_{\text{Ulac}},\ j \in N^{\text{ER},m}_{\text{Uac}} \tag{39}$$

2) Constraints of R-layer and its new DC lines

Each port of R-layer and its corresponding new DC electric line should be deployed together. Since the port of R-layer can be a parent bus or a child bus, the relationship between the port of R-layer and its new DC electric line is identified by connecting resistance in (40)–(41).

$$\pi^{\text{ER},m}_{\text{Rdc},i} \le N^{\max}_{\text{Rdc}} \delta^{\text{ER},m}_{\text{Rdc},j},\ r_{i,j} \ne 0,\ i \in N^{\text{ER},m}_{\text{Rdc}},\ j \in N^{\text{ER},m}_{\text{Rldc}} \tag{40}$$

$$\delta^{\text{ER},m}_{\text{Rdc},j} \le \pi^{\text{ER},m}_{\text{Rdc},i},\ r_{i,j} \ne 0,\ i \in N^{\text{ER},m}_{\text{Rdc}},\ j \in N^{\text{ER},m}_{\text{Rldc}} \tag{41}$$

Similarly, only when the new DC electric lines and ports of R-layer are built, can branch currents be allowed.

$$\begin{cases} \sum_{i\to j} I^2_{ij,s} \le M_1 \delta^{\text{ER},m}_{\text{Rdc},i}, & \text{if } i \in N^{\text{ER},m}_{\text{Rldc}} \\ \sum_{i\to j} I^2_{ij,s} \le M_1 \delta^{\text{ER},m}_{\text{Rdc},j}, & \text{if } j \in N^{\text{ER},m}_{\text{Rldc}} \end{cases} \tag{42}$$

$$\begin{cases} \sum_{i\to j} I^2_{ij,s} \le M_2 \pi^{\text{ER},m}_{\text{Rdc},i}, & \text{if } i \in N^{\text{ER},m}_{\text{Rdc}} \\ \sum_{i\to j} I^2_{ij,s} \le M_2 \pi^{\text{ER},m}_{\text{Rdc},j}, & \text{if } j \in N^{\text{ER},m}_{\text{Rdc}} \end{cases} \tag{43}$$

3) Special operational constraints of R-layer

As designed above, R-layer is only used for energy transactions between its own DN and other DNs, and F-layer helps to forward the trading energy of other DNs. Thus, power flow directions of ports at R-layer should be limited to be the same in each scenario s. Such a process is modeled by adding binary variables in (44) in this paper.

$$\begin{cases} P^{\text{ER},m}_{\text{Rdc},j,s} \le M_3 \delta^{\text{ER},m}_{\text{Rdcp},s}, & j \in N^{\text{ER},m}_{\text{Rdc}} \\ P^{\text{ER},m}_{\text{Rdc},j,s} \ge M_3 (\delta^{\text{ER},m}_{\text{Rdcp},s} - 1), & j \in N^{\text{ER},m}_{\text{Rdc}} \end{cases} \tag{44}$$

4) Special operational constraints of DN m

For ensuring willingness of energy sharing among DNs, a P2P energy transaction should not impair the benefit of any individual DN first. In other words, only when there is surplus energy in DN_m, can energy of DN_m be sold to other DNs through R-layer. Meanwhile, only when an energy shortage occurs in DN_m, can energy is purchased from other DNs through R-layer. Thus, in DN_m, energy exchanging directions with the upstream grid and with other DNs in the P2P market should be limited to the same by (45).

$$\begin{cases} P_{ig,s} \le M_4 \delta^{\text{ER},m}_{\text{Rdcp},s}, & i \in N^{\text{slack},m}_{\text{ac}} \\ P_{ig,s} \ge M_4 (\delta^{\text{ER},m}_{\text{Rdcp},s} - 1), & i \in N^{\text{slack},m}_{\text{ac}} \end{cases} \tag{45}$$

5) Constraints of F-layer

Only when ports of F-layer are configured, can branch current be allowed.

$$\sum_{i:i\to j} I^2_{ij} \le M_5 \pi^{\text{ER},m}_{\text{Fdc},j,s},\ i \in N^{\text{ER},m}_{\text{Fldc}},\ j \in N^{\text{ER},m}_{\text{Fdc}} \tag{46}$$

C. Modeling of a P2P Energy Transaction

According to the modeling process in [32], [33], conventional P2P energy transactions mainly include two parts: a) designing a mechanism of P2P clearing price; b) purchasing energy should be strictly the same as selling energy at any dispatching period.

1) The mechanism of P2P clearing price

In this paper, two kinds of *mechanisms will be implemented to test the proposed planning model.*

2) Fixed gap based clearing price

In this mechanism, clearing price is floating within the price provided by the upstream grid, and ignores the state of energy balance among DNs. The fixed gap based mechanism is shown in (47), and $0 < \beta < 1$. The P2P trader will benefit more along with decreasing β.

$$\begin{cases} C_{\mathrm{p2p},s}^{\mathrm{sell},m} = C_{\mathrm{up},s}^{\mathrm{sell}} + \beta \frac{C_{\mathrm{up},s}^{\mathrm{buy}} - C_{\mathrm{up},s}^{\mathrm{sell}}}{2} \\ C_{\mathrm{p2p},s}^{\mathrm{buy},m} = C_{\mathrm{up},s}^{\mathrm{buy}} - \beta \frac{C_{\mathrm{up},s}^{\mathrm{buy}} - C_{\mathrm{up},s}^{\mathrm{sell}}}{2} \end{cases} \tag{47}$$

3) SDR based clearing price

The SDR based mechanism considers the relationship between supply and demand in the entire system [32], [33]. More surplus energy means a lower trading price; otherwise, a higher trading price will be made. First, supply and demand relationship (SDR) is calculated by (48)–(50).

$$SDR_s = TSP_s / TDP_s \tag{48}$$

$$NP_s = \sum_{m=1}^{N^{\mathrm{DN}}} \left(P_{dj,s} + P_{\mathrm{netloss}}^{m} - P_{ig,s} \right), \quad j \in N_{\mathrm{ac}}^{\mathrm{bus},m},\ i \in N_{\mathrm{ac}}^{\mathrm{DG},m} \tag{49}$$

$$\begin{cases} TSP_s = -NP_s, & \text{if } NP_s < 0 \\ TDP_s = NP_s, & \text{else} \end{cases} \tag{50}$$

The SDR based clearing price is carried out by (51)–(52).

$$C_{\mathrm{p2p},s}^{\mathrm{sell},m} = \begin{cases} \frac{(C_{\mathrm{up},s}^{\mathrm{sell}} + \alpha_1) \cdot (C_{\mathrm{up},s}^{\mathrm{buy}} - \alpha_2)}{(C_{\mathrm{up},s}^{\mathrm{buy}} - \alpha_2 - C_{\mathrm{up},s}^{\mathrm{sell}} - \alpha_1) SDR_s + C_{\mathrm{up},s}^{\mathrm{sell}} + \alpha_1}, \\ \qquad\qquad 0 \le SDR_s \le 1 \\ C_{\mathrm{up},s}^{\mathrm{sell}} + \alpha_1, \qquad SDR_s > 1 \end{cases} \tag{51}$$

$$C_{\mathrm{p2p},s}^{\mathrm{buy},m} = \begin{cases} (C_{\mathrm{up},s}^{\mathrm{buy}} - \alpha_2)(1 - SDR_s) \\ \quad + (C_{\mathrm{p2p},s}^{\mathrm{sell},m}) SDR_s + \alpha_3, \quad 0 \le SDR_s \le 1 \\ C_{\mathrm{p2p},s}^{\mathrm{sell},m} + \alpha_3, \qquad SDR_s > 1 \end{cases} \tag{52}$$

Considering the price of the upstream grid, a_1, a_2 and a_3 are additionally added to ensure the P2P energy transaction is still attractive. When SDR is high, a_1 ensures that surplus energy sold in the P2P market gains more profit. a_2 ensures that demand met in the P2P market has less cost when SDR is low. a_3 ensures the P2P trader has profit when the SDR is high or low. The SDR based mechanism is shown in Fig. 4.

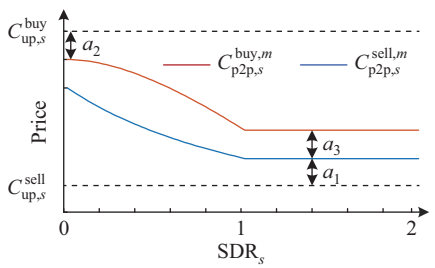

Fig. 4. The SDR based clearing price.

4) The DC network for P2P energy balance

In this paper, the transferring energy of P2P transactions is implemented through P2P-based DC electric lines and ERs. Thus, P2P energy balance will be met if the power flow constraints of the P2P-based DC network are met. A power flow calculation model combined with R-layer and F-layer is shown in (53)–(55).

$$\sum_{i:i\to j} (P_{ij,s} - r_{ij} I_{ij,s}^2) + P_{gj,s} = \sum_{j \in N_{\mathrm{Rdc}}^{\mathrm{ER},m}} P_{\mathrm{Rdc},j,s}^{\mathrm{ER},m} + \sum_{j \in N_{\mathrm{Fdc}}^{\mathrm{ER},m}} P_{\mathrm{Fdc},j,s}^{\mathrm{ER},m} + P_{dj,s} + \sum_{k:j\to k} P_{jk,s},\ i,\ j,k \in N_{\mathrm{dc}}^{\mathrm{bus}} \tag{53}$$

$$U_{j,s}^2 = U_{i,s}^2 - 2 r_{ij} P_{ij,s} + I_{ij,s}^2 r_{ij}^2,\ i \to j,\ i,j \in N_{\mathrm{dc}}^{\mathrm{bus}} \tag{54}$$

$$U_{i,s}^2 I_{ij,s}^2 = P_{ij,s}^2,\ i \to j,\ i,j \in N_{\mathrm{dc}}^{\mathrm{bus}} \tag{55}$$

Line capacity limit, branch current limit and voltage limit constraints are shown in (56)–(58), respectively.

$$-S_{ij}^{\mathrm{N}} \le P_{ij,s} \le S_{ij}^{\mathrm{N}},\ i,j \in N_{\mathrm{dc}}^{\mathrm{bus}} \tag{56}$$

$$I_{ij}^{\mathrm{L}} \le I_{ij,s} \le I_{ij}^{\mathrm{H}},\ i,j \in N_{\mathrm{dc}}^{\mathrm{bus}} \tag{57}$$

$$U_i^{\mathrm{L}} \le U_{i,s} \le U_i^{\mathrm{H}},\ i \in N_{\mathrm{dc}}^{\mathrm{bus}} \tag{58}$$

D. AC Power Flow Calculation Model of DN_m

A power flow model of the AC network in DN_m is conventional. Equality constraints are shown in (59)–(62).

$$\sum_{i:i\to j} \left(P_{ij,s} - r_{ij} I_{ij,s}^2 \right) + P_{gj,s} = P_{dj,s} + \sum_{k:j\to k} P_{jk,s},\quad i,\ j \in N_{\mathrm{ac}}^{\mathrm{bus},m} \tag{59}$$

$$\sum_{i:i\to j} (Q_{ij,s} - x_{ij} I_{ij,s}^2) + Q_{gj,s} = Q_{dj,s} + \sum_{k:j\to k} Q_{jk,s},\quad i,\ j \in N_{\mathrm{ac}}^{\mathrm{bus},m} \tag{60}$$

$$U_{j,s}^2 = U_{i,s}^2 - 2(r_{ij} P_{ij,s} + x_{ij} Q_{ij,s}) + I_{ij,s}^2 z_{ij}^2,\quad i \to j,\ i,j \in N_{\mathrm{ac}}^{\mathrm{bus},m} \tag{61}$$

$$U_{i,s}^2 I_{ij,s}^2 = P_{ij,s}^2 + Q_{ij,s}^2,\ i \to j,\ i,j \in N_{\mathrm{ac}}^{\mathrm{bus},m} \tag{62}$$

Line capacity limit, branch current limit and voltage limit constraints are shown in (63)–(65), respectively.

$$(P_{ij,s})^2 + (Q_{ij,s})^2 \le (S_{ij}^{\mathrm{N}})^2,\ i,j \in N_{\mathrm{ac}}^{\mathrm{bus},m} \tag{63}$$

$$I_{ij}^{\mathrm{L}} \le I_{ij,s} \le I_{ij}^{\mathrm{H}},\ i,\ j,k \in N_{\mathrm{ac}}^{\mathrm{bus},m} \tag{64}$$

$$U_i^{\mathrm{L}} \le U_{i,s} \le U_i^{\mathrm{H}},\ i \in N_{\mathrm{ac}}^{\mathrm{bus},m} \tag{65}$$

E. The MISOCP-based Planning Model Conversion

Assume that N^{DN} DNs participate in the P2P energy transaction market. Then, the total cost of N^{DN} DNs is shown in (66), and is the final objective function of the proposed planning model in this paper. Decision variables are the capacity of ports at U-layer, R-layer and F-layer in each ER. Variables controlling construction of new AC and DC electric lines are also decision variables. Therefore, in this paper, the proposed planning model of energy routers considering P2P

energy transactions among multiple DNs is entirely shown in (1)–(66).

$$\min f_{\rm sys} = \sum_{m=1}^{N^{\rm DN}} f_m \left(\pi_{{\rm Uac},j}^{{\rm ER},m}, \pi_{{\rm Rdc},j}^{{\rm ER},m}, \pi_{{\rm Fdc},j}^{{\rm ER},m}, \delta_{{\rm Uac},j}^{{\rm ER},m}, \delta_{{\rm Rdc},j}^{{\rm ER},m}\right) \tag{66}$$

For linearizing the proposed planning model, variables $U_{j,s}^2$ and $I_{ij,s}^2$ in the above equality and inequality constraints are denoted as $\hat{U}_{j,s}$ and $\hat{I}_{ij,s}$, respectively. However, the model is still nonlinear because of equality constraints (4), (9), (55) and (62). Capacity limit constraints are second-order cones such as (63). For solving the planning model in a way of conic programming, equality constraints (4), (9), (55) and (62) are relaxed as rotated quadratic cones shown in (67)–(70), respectively. Thus, the planning model is converted as a MISOCP-based model, and can be solved by commercial solvers such as XPRESS and CPLEX. The detailed relaxation process refers to [29], and the detailed model is in Appendix A.

$$\hat{U}_{j,s}\hat{I}_{ij,s} \geq P_{ij,s}^2 + Q_{ij,s}^2,\ i \to j,\ i \in N_{\rm Ulac}^{{\rm ER},m},\ j \in N_{\rm Uac}^{{\rm ER},m} \tag{67}$$

$$\hat{U}_{j,s}\hat{I}_{ij,s} \geq P_{ij,s}^2 + Q_{ij,s}^2,\ i \to j,\ i \in N_{\rm ac}^{{\rm ER},m},\ j \in N_{\rm Ulac}^{{\rm ER},m} \tag{68}$$

$$\hat{U}_{j,s}\hat{I}_{ij,s} \geq P_{ij,s}^2,\ i \to j,\ i,j \in N_{\rm dc}^{\rm bus} \tag{69}$$

$$\hat{U}_{j,s}\hat{I}_{ij,s} \geq P_{ij,s}^2 + Q_{ij,s}^2,\ i \to j,\ i,j \in N_{\rm ac}^{{\rm bus},m} \tag{70}$$

F. Evaluation Indexes of the Planning Results

Five indexes are set to evaluate derived results: a) total cost $f_{\rm sys}$ of all DNs; b) comprehensive cost f_m of ${\rm DN}_m$; c) power volatility $K_{{\rm var}\_m}$ between ${\rm DN}_m$ and its upstream grid; d) voltage deviation $K_{{\rm vol}\_m}$ of ${\rm DN}_m$; e) relaxation gap indexes $K_{{\rm gap}\_m}$ and $K_{\rm gapdc}$ of AC and DC network, respectively. Smaller relaxation gaps indicate that relaxed equalities are tight in the MISOCP-based model and derived solutions are those of the original planning problem. $f_{\rm sys}$ and f_m refer to (66) and (15), respectively. The rest are shown in (71)–(74).

$$K_{{\rm var}\_m} = \frac{1}{N_s}\sum_{s=1}^{s=N_s}\left(P_{ig,s} - \sum_{s=1}^{s=N_s}\frac{P_{ig,s}}{N_s}\right)^2,\ i \in N_{\rm ac}^{{\rm slack},m} \tag{71}$$

$$K_{{\rm vol}\_m} = \sqrt{\sum_{s=1}^{s=N_s}\sum_{i}(U_{i,s}-1)^2/(N_{\rm bus}^m N_s)},\ i \in N_{\rm ac}^{{\rm bus},m} \tag{72}$$

$$K_{{\rm gap}\_m} = \max_{i\to j,s,m}\left\{\left|\hat{U}_{j,s}\hat{I}_{ij,s} - P_{ij,s}^2 - Q_{ij,s}^2\right|\right\},\ i,\ j \in N_{\rm ac}^{{\rm bus},m} \cup N_{\rm Ulac}^{{\rm ER},m} \cup N_{\rm Uac}^{{\rm ER},m} \tag{73}$$

$$K_{\rm gapdc} = \max_{i\to j,s}\left\{\left|\hat{U}_{j,s}\hat{I}_{ij,s} - P_{ij,s}^2 - Q_{ij,s}^2\right|\right\},\ i,j \in N_{\rm dc}^{\rm bus} \tag{74}$$

IV. CASE STUDY

To verify effectiveness of the proposed planning model, four IEEE-33 systems-based hybrid systems is taken as the test benchmark shown in Fig. 5. The four AC systems are ${\rm DN}_1$∼${\rm DN}_4$, respectively. Each AC system contains 41 buses, i.e., bus 1∼41. For example, bus indexes in ${\rm DN}_1$ are ${\rm bA}_1$∼${\rm bA}_{41}$. Bus indexes of the other DNs are prefixed with bB, bC and bD, respectively, and the number of buses is consistent. For the DC system, candidate buses are ${\rm dC}_1$∼${\rm dC}_{48}$, and the prefix is dC. Therefore, the total initial bus number of AC and DC systems is 212. Impedance and load parameters of the IEEE-33 system are from Matpower 7.0. The base capacity is 10 MVA, and base voltage is 12.66 kV. Total active load is 3.715 MW, and reactive load is 2.3 Mvar.

Each DN is equipped with an ER. Each ER has four candidate ports at U-layer, three candidate ports at R-layer and F-layer. For example, in ${\rm DN}_1$, candidate ports of U-layer of ${\rm ER}_1$ are ${\rm bA}_{35}$, ${\rm bA}_{37}$, ${\rm bA}_{39}$ and ${\rm bA}_{41}$, and candidate ports of R-layer are ${\rm dC}_1$, ${\rm dC}_3$ and ${\rm dC}_5$. F-layer is placed between the ports of R-layer. Only one end of the converter at F-layer is stated to denote the port at F-layer. Thus, candidate ports are ${\rm dC}_7$, ${\rm dC}_9$ and ${\rm dC}_{11}$.

The main simulation parameters are shown in Table I [20], [23], [29], [34], [35]. New AC electric lines are laid based on the path with minimum total resistance of the existing line (including the tie switch branch). Impedances of the new AC lines are the sum of the impedances of existing lines on those paths. Unit resistance of the new line is set as 0.3 Ω/km, and length of the new line is roughly estimated by total resistance of the new line. Connection resistance of between the energy router itself and its locating bus is set to 0.001 Ω, ignoring reactance. Meanwhile, for a branch with no impedance between the port of the ER and bus in Fig. 5, 0.001 Ω is set as the connection resistance.

Table II shows the parameters of candidate AC and DC lines. For example, in ${\rm DN}_1$, ${\rm ER}_1$ itself is placed beside bus ${\rm bA}_{29}$. Impedance of line ${\rm L}_{29,38}$ between the port of U-layer and bus ${\rm bA}_{29}$ is almost 0, and 0.001 is set as the connection impedance of the port at U-layer. Similarly, in ${\rm DN}_2$, ${\rm ER}_2$ itself is placed beside bus ${\rm bB}_{33}$. Impedance of line ${\rm L}_{18,34}$ between U-layer and bus ${\rm bB}_{33}$ is almost 0, and 0.001 is set as the connection impedance of the port at U-layer. In the DC system, equivalent resistances of ports at R-layer and F-layer are 0.0321 Ω, and six candidate DC lines are listed.

For the IEEE-33 system, buses with PVs are bus 7, 13 and 27, and the rated capacities are 500, 300 and 400 kVA,

TABLE I
THE MAIN PARAMETERS CONFIGURATION

Parameter	Value	Parameter	Value	Parameter	Value
$T_{\rm h}$	1095	$y_{\rm ac}$, $y_{\rm dc1}$, $y_{\rm dc2}$	20	$\lambda_{\rm P}$(¥/kWh)	0.3
$S_{\rm ac}^{\rm ER}, S_{\rm dc}^{\rm ER}$ (kVA)	50	$C_{\rm Uac}^U, C_{\rm Rdc}^U, C_{\rm Fdc}^U$ (¥/kVA)	800	$\xi_{\rm Uac}, \xi_{\rm Rdc}, \xi_{\rm Fdc}$	0.01
$x_{\rm er}$ (Ω)	0.539	$r_{\rm er}$ (Ω)	0.0321	$d_{\rm ac}, d_{\rm dc1}, d_{\rm dc2}$	0.08
$\phi_{\rm ac}, \phi_{\rm dc}$	20	$\tau_{\rm ac}, \tau_{\rm dc}$	0.08	$C_{\rm pac}^{\rm line}$ (¥/km)	9600

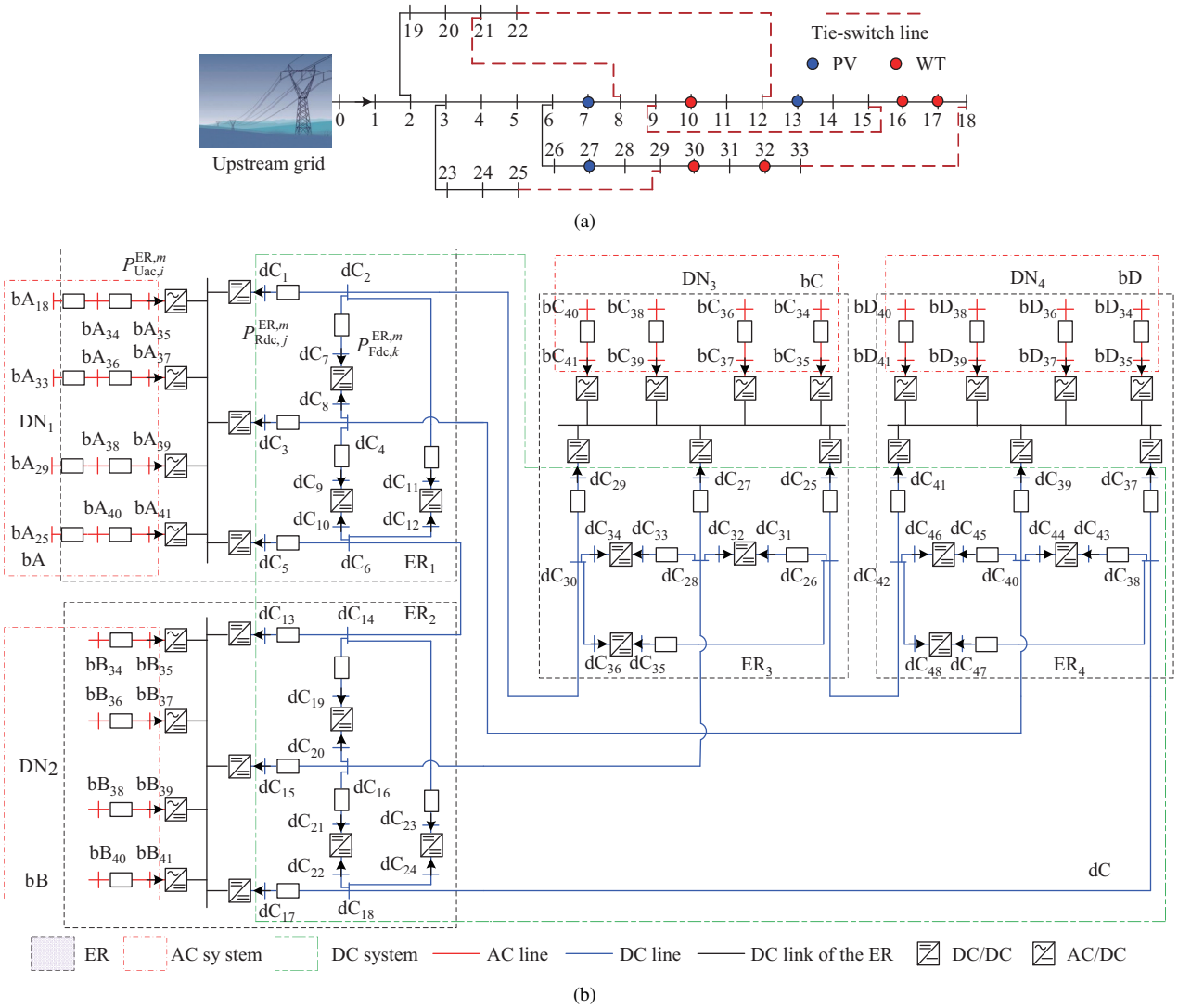

Fig. 5. The modified structure of the ERs-based IEEE-33. (a) The IEEE-33 system based DN. (b) The ERs-based DNs system with P2P interconnection.

TABLE II
PARAMETERS OF CANDIDATE NEW ELECTRIC LINES IN AC AND DC SYSTEM

AC system (prefixed by bA, bB, bC and bD)							
ER_1 is beside bus bA_{29} in DN_1		ER_2 is beside bus bB_{33} in DN_2		ER_3 is beside bus bC_{18} in DN_3		ER_4 is beside bus bD_{29} in DN_4	
Candidate lines	Impedance (Ω)	Candidate lines	Impedance (Ω)	Candidate lines	Impedance (Ω)	Candidate lines	Impedance (Ω)
$L_{18,34}$	2.63+j2.61	$L_{18,34}$	0.5+j0.5	$L_{18,34}$	0.001	$L_{18,34}$	2.63+j2.61
$L_{25,40}$	0.5+j0.5	$L_{25,40}$	2.63+j2.61	$L_{25,40}$	3.13+j3.11	$L_{25,40}$	0.5+j0.5
$L_{29,38}$	0.001	$L_{29,38}$	2.13+j2.11	$L_{29,38}$	2.63+j2.61	$L_{29,38}$	0.001
$L_{33,36}$	2.13+j2.11	$L_{33,36}$	0.001	$L_{33,36}$	0.5+j0.5	$L_{33,36}$	2.13+j2.11
DC system (prefixed by dC)							
Candidate lines	Resistance (Ω)	Candidate lines	Resistance (Ω)	Candidate lines	Resistance (Ω)	–	–
$L_{2,30}$	3	$L_{6,14}$	2.5	$L_{18,38}$	7	–	–
$L_{4,40}$	6.5	$L_{16,28}$	2	$L_{26,42}$	3.5	–	–

respectively. Buses with WTs are bus 10, 16, 17, 30 and 32, and rated capacities are 500, 200, 150, 200 and 300 kVA, respectively [29]. Different capacity coefficients will be tested.

Multiple scenarios are considered in this paper to evaluate variations of load and distributed generation. How many scenarios should be selected depends on practical requirements. In [29], the number of selected scenarios derived according to probability is twenty-five. If the optimization problem contains energy storage devices, the multiple scenarios should be time-sequential, and duration is usually 24 hours [36]. If variations of the load and renewable energy will be ignored, then only one scenario will be selected.

In this paper, eight scenarios are derived from a typical day. Curves of load, PV and WT are obtained by superposition of typical output curves and random fluctuations. Considering that the planning model with four distribution systems is relatively complex in the case study, this paper simplifies data and prices of a typical day in 24 hours [3]. As shown in Fig. 6,

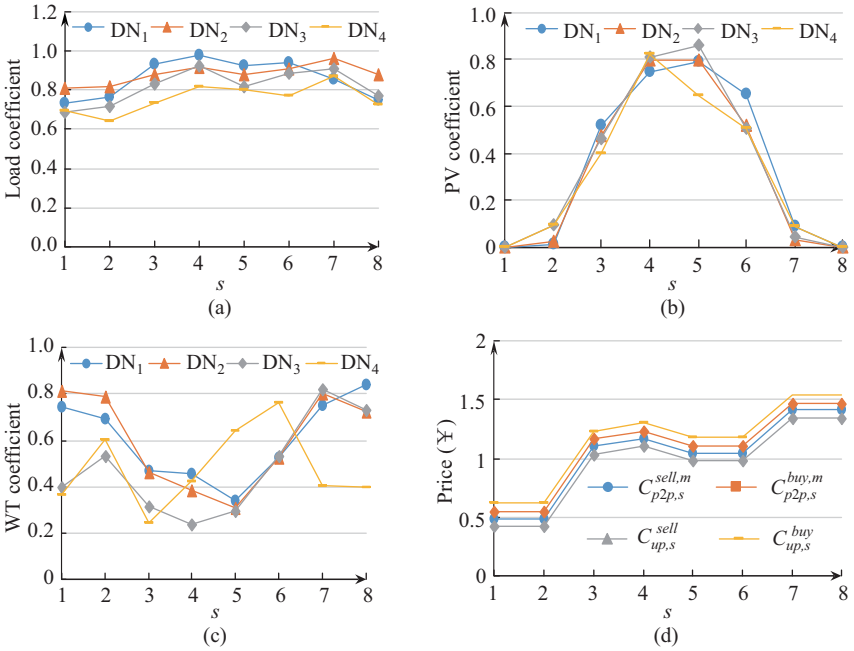

Fig. 6. The reduced 8 typical scenarios in four DNs. (a) The load curve. (b) The output of PV. (c) The output of WT. (d) The trading price in both markets.

eight scenarios are obtained by averaging every three adjacent data to denote a typical day. Each scenario is represented by one point of data. In Fig. 6, eight points of data represent eight scenarios. Such a definition is similar to [29] and different from [30]. In [30], each scenario contains 24 points of data. The number of scenarios will not impair the generality of the proposed model in this paper [29].

The MISOCP-based planning model is solved by the XPRESS solver in GAMS 28.2.0 platform. The computer configuration is "i7-6700 CPU@3.40 GHz (8 GB RAM)".

A. Effectiveness Verification of the Proposed Planning Model

A fixed gap based clearing price is adopted in Case A, and electric prices in both markets are shown in Fig. 6(d).

Three subcases are conducted: A1) regular operation of four DNs without any ER; A2) operation of the ERs-based DNs system without P2P energy transactions; A3) operation of the ERs-based DNs system with P2P energy transactions. Thus, in subcase A2, operation of ER is similar to that of SOP. Allocation differences between SOP and ER can be concluded from results in subcase A2 and A3. The capacity coefficient of DG in each DN is shown in Table III. DN_1 is a PV town, and DN_2 is a WT town. DN_3 and DN_4 have PV and WT, but DN_4 only has the basic configuration of DG.

TABLE III
THE CAPACITY CONFIGURATIONS OF EACH DN IN CASE A

Generator Type	DN_1	DN_2	DN_3	DN_4
PV	5	0	3.5	1
WT	0	5	4	1

1) Analysis of the Derived Schemes of ERs

The derived schemes of ERs in A2 and A3 are shown in Tables IV and V. In A2 and A3, four candidate ports of the U-layer of four ERs are all configured. Thus, all four candidate new AC electric lines at each DN will be built for connection of U-layer. In A3, port capacities of U-layer increase slightly as a whole, compared with those in A2. For example, in A2, ports of U-layer in ER_1 are bA_{35}, bA_{37}, bA_{39} and bA_{41}, and capacities are 350, 200, 800 and 650 kVA, respectively. In A3, corresponding port capacities of ER_1 become 450, 200, 1000 and 400 kVA, respectively.

For R-layer in A3, in ER_1, only port dC_5 is configured among candidate ports dC_1, dC_3 and dC_5, and configuration capacity is 1550 kVA. Thus, new candidate DC lines excluding $L_{2,30}$ and $L_{4,40}$ will be built in the DC system. For F-layer, capacity configuration of candidate ports dC_7, dC_9 and dC_{11}

TABLE IV
CONFIGURATION RESULTS OF ERS IN SUBCASE A2

ER_1 (kVA)	ER_2 (kVA)	ER_3 (kVA)	ER_4 (kVA)
Port capacity of U-layer			
bA_{35} (350)	bB_{35} (900)	bC_{35} (700)	bD_{35} (200)
bA_{37} (200)	bB_{37} (650)	bC_{37} (500)	bD_{37} (200)
bA_{39} (800)	bB_{39} (400)	bC_{39} (300)	bD_{39} (650)
bA_{41} (650)	bB_{41} (1100)	bC_{41} (900)	bD_{41} (300)

TABLE V
CAPACITY CONFIGURATIONS OF ERS IN SUBCASE A3

ER_1 (kVA)	ER_2 (kVA)	ER_3 (kVA)	ER_4 (kVA)
Port capacity of the U-layer			
bA_{35} (450)	bB_{35} (1400)	bC_{35} (950)	bD_{35} (200)
bA_{37} (200)	bB_{37} (950)	bC_{37} (550)	bD_{37} (200)
bA_{39} (1000)	bB_{39} (500)	bC_{39} (550)	bD_{39} (900)
bA_{41} (400)	bB_{41} (700)	bC_{41} (550)	bD_{41} (700)
Port capacity of R-layer			
dC_1 (0)	dC_{13} (1600)	dC_{25} (1200)	dC_{37} (500)
dC_3 (0)	dC_{15} (250)	dC_{27} (200)	dC_{39} (0)
dC_5 (1550)	dC_{17} (600)	dC_{29} (0)	dC_{41} (1000)
Port capacity of F-layer			
dC_7 (0)	dC_{19} (0)	dC_{31} (0)	dC_{43} (0)
dC_9 (0)	dC_{21} (150)	dC_{33} (0)	dC_{45} (0)
dC_{11} (0)	dC_{23} (50)	dC_{35} (0)	dC_{47} (150)

in the ER_1 are 0, which means they will not be deployed. F-layer of ER_2 is configured with ports dC_{21} and dC_{23}, with a capacity of 150 and 50 kVA, respectively. Besides, port dC_{47} is configured in F-layer of ER_4.

Note the configuration capacity of two interconnection ports may not be the same. For example, ports dC_5 and dC_{13} have one step capacity differences. That is reasonable because line loss is significant under considerable exchanging energy, and the step capacity is 50 kVA. Besides, F-layer can realize capacity sharing of R-layer in the same ER. Such a process will be analyzed in the P2P transaction part.

Relaxing gap indexes are shown in Table VI. Most of the maximum relaxation gaps of the three subcases are within error 1e-6, which means the relaxing equalities are tight [37]. Thus, derived results of the three subcases are effective.

Therefore, the above simulation results verify the proposed planning model can obtain configuring schemes of ERs for the P2P energy sharing among multiple DNs.

2) Comprehensive cost analysis of the DN

In A2, f_{sys} is 1.880e7 ¥, and is 11.40% lower than in A1. Cost reduction means that configuring ER can bring loss reduction in DN and benefits increase. For example, when DN_2 is not equipped with ER_2 in A1, f_2 is −0.222e7 ¥, which means revenue is 0.222e7 ¥. For operation of DN_2 in A2, f_2 is −0.318e7 ¥, and the increase rate is 43.24%.

In A3, f_{sys} is 1.597e7 ¥, which is 24.74% lower than in A1. Thus, P2P energy transactions bring the best benefits for the ERs-based DNs system. For operation of DN_2 in A3, f_2 is −0.400e7 ¥, and the increase rate is 80.18%.

Compared with A2, cost reduction rates of f_1 and f_4 in A3 are 6.07% and 2.91%, respectively. Revenue increase rates of f_2 and f_3 in A3 are up to 36.94% and 9.35%, respectively. Such results show that each participating DN gains benefit from P2P energy transactions. Besides, according to results shown in Fig. 7(b) and 7 (c), DN_2 and DN_3 mainly sell surplus energy in the P2P market, and DN_1 and DN_4 mainly purchase energy. Such results show that energy sellers benefit more from the P2P market.

Thus, the simulation results show that configuration of ER can reduce the total cost of DNs. All participating DNs can benefit from ERs-based P2P energy transactions, and DNs with more surplus energy benefit more.

3) Volatility analysis of exchanging power with the upstream grid

In Table VI, volatility K_{var} of exchanging power in A2 increases slightly as a whole because the ER reduces network loss of the DN. Thus, demand from the upstream grid is reduced, or more surplus energy is sold. For example, the power curve of DN_2 in Fig. 7(b) in s_1 moves down compared with that in Fig. 7(a). Selling power between DN_2 and its upstream grid in s_1 in A1 and A2 are 2128 and 2300 kW, respectively. Meanwhile, at s_5, the power curve of DN_2 in Fig. 7(b) moves down compared with that in Fig. 7(a). The purchasing powers between DN_2 and the upstream grid at s_5 in A1 and A2 are 1256 and 1208 kW, respectively.

As shown in Fig. 7(c) and Table VI, excluding DN_4, power volatility between the DN and upstream grid is significantly reduced in A3. Direct consumption of surplus energy of the DG is achieved among DNs with the same rated voltage, and overall adverse impact of DNs on the upstream grid is significantly alleviated. $K_{\text{var\_4}}$ of DN_4 increases, but exchanging power of DN_4 decreases, obviously. At s_5 and s_6, purchasing power of DN_4 is almost reduced to 0. Besides, peak-valley power differences of DN_4 in A1 and A3 are 1416 and 1485 kW, respectively. They are almost the same. Therefore, in A3, DN_4 does not increase the regulatory burden of the upstream grid.

Therefore, simulation results verify that exchanging power volatility between DNs and their upstream grids is significantly reduced as a whole by the proposed ERs-based P2P system. Besides, surplus energy of DG is consumed among ERs-based DNs with the same rated voltage directly.

TABLE VI
EVALUATION INDEXES OF SIMULATION RESULTS IN CASE A

Subcase	f_{sys} (¥)	f_1 (¥)	f_2 (¥)	f_3 (¥)	f_4 (¥)	$K_{\text{var\_1}}$	$K_{\text{var\_2}}$	$K_{\text{var\_3}}$	$K_{\text{var\_4}}$
A1	2.122e7	1.186e7	−0.222e7	−0.770e7	1.927e7	2.825	1.528	0.456	0.215
A2	1.880e7	1.140e7	−0.318e7	−0.841e7	1.899e7	2.864	1.652	0.484	0.212
A3	1.597e7	1.068e7	−0.400e7	−0.913e7	1.843e7	0.422	0.005	0.085	0.345
Subcase	$K_{\text{vol\_1}}$	$K_{\text{vol\_2}}$	$K_{\text{vol\_3}}$	$K_{\text{vol\_4}}$	$K_{\text{gap\_1}}$	$K_{\text{gap\_2}}$	$K_{\text{gap\_3}}$	$K_{\text{gap\_4}}$	K_{gapdc}
A1	0.032	0.036	0.026	0.027	2.9e-7	3.3e-7	3.1e-7	2.7e-7	–
A2	0.019	0.029	0.022	0.014	9.3e-6	1.1e-5	1.0e-5	9.0e-6	–
A3	0.009	0.015	0.012	0.008	3.4e-6	3.5e-6	3.5e-6	3.4e-6	5.2e-6

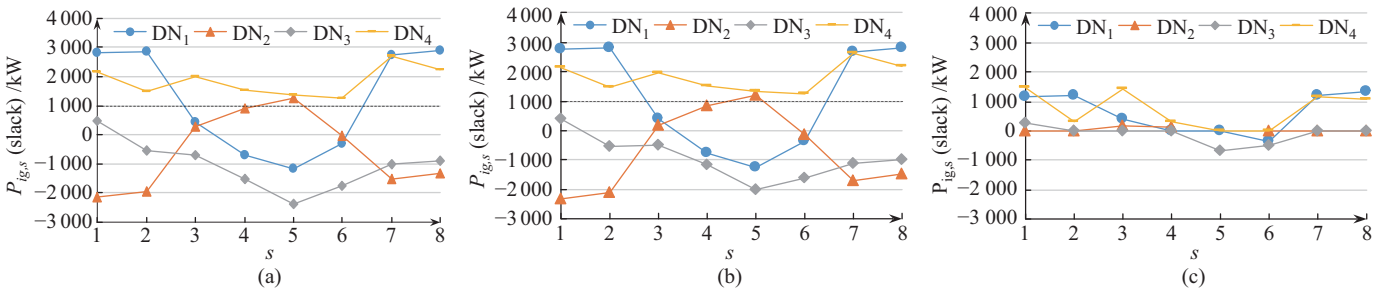

Fig. 7. The exchanging power between four DNs and their upstream grids: (a) results in A1; (b) results in A2; (c) results in A3.

4) The voltage deviation in the DN

In Table VI, voltage deviation indexes are significantly reduced by configuring ER in A2 and A3, and ERs-based P2P energy sharing in A3 performs best. Voltage curves of four DNs in A1, A2 and A3 are shown in Figs. 8–11, respectively. In Fig. 9(a), in s_1, some bus voltages of DN_2 reach the upper limit of 1.1 p.u., which violates requirements of safety operation. Thus, some outputs of WTs in DN_2 should be abandoned to recover the bus voltages.

In A3, bus voltages of the four DNs are all close to 1 p.u. as a whole, and overall deviation is the smallest. Thus, power quality of the DNs is effectively improved. Especially, outputs of WTs in DN_2 are not required to cut in A3.

Therefore, simulation results verify the proposed ERs-based P2P energy trading between DNs can effectively reduce voltage deviation of the DN, improve power quality of the DN, and promote consumption of DG.

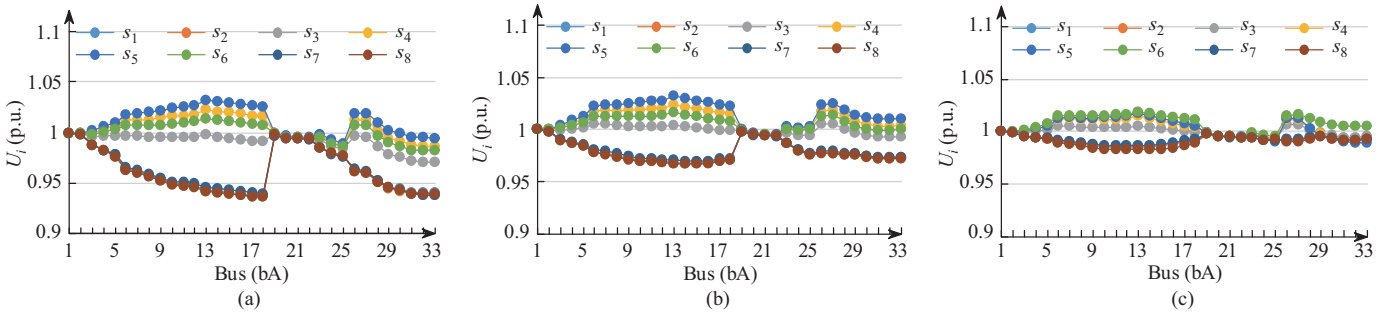

Fig. 8. The bus voltages of DN_1 in different subcases. (a) Results in A1. (b) Results in A2. (c) Results in A3.

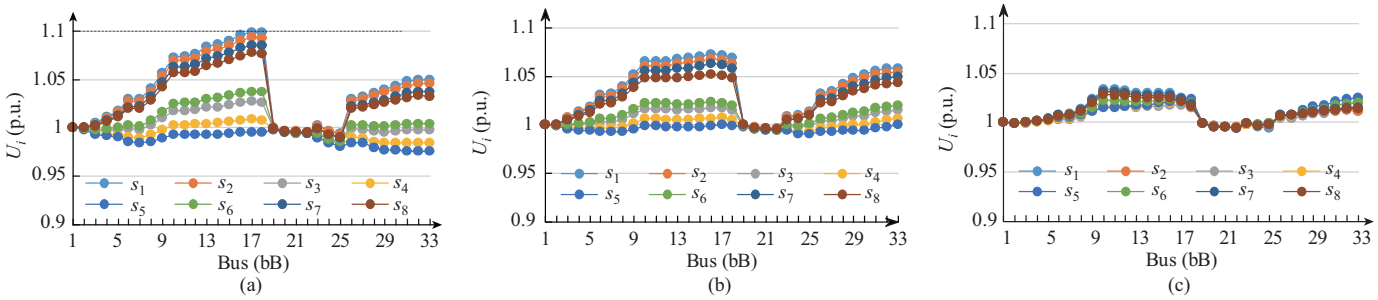

Fig. 9. The bus voltages of DN_2 in different subcases. (a) Results in A1. (b) Results in A2. (c) Results in A3.

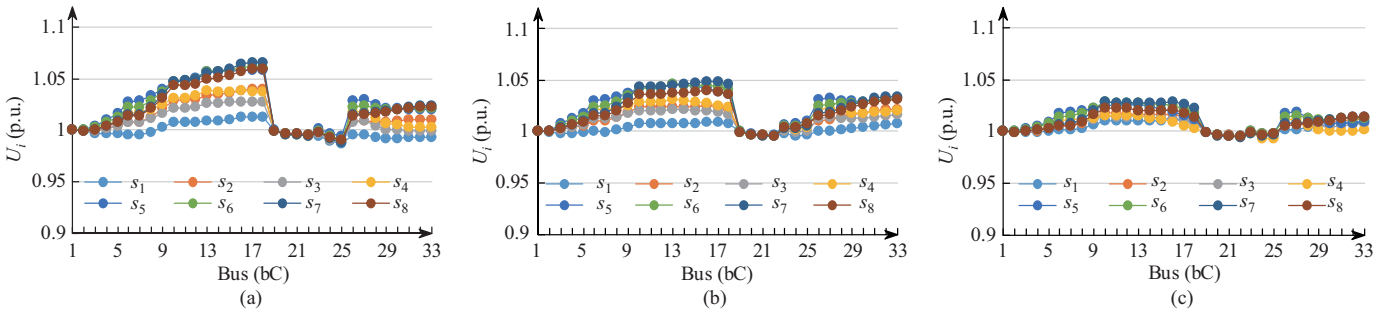

Fig. 10. The bus voltages of DN_3 in different subcases. (a) Results in A1. (b) Results in A2. (c) Results in A3.

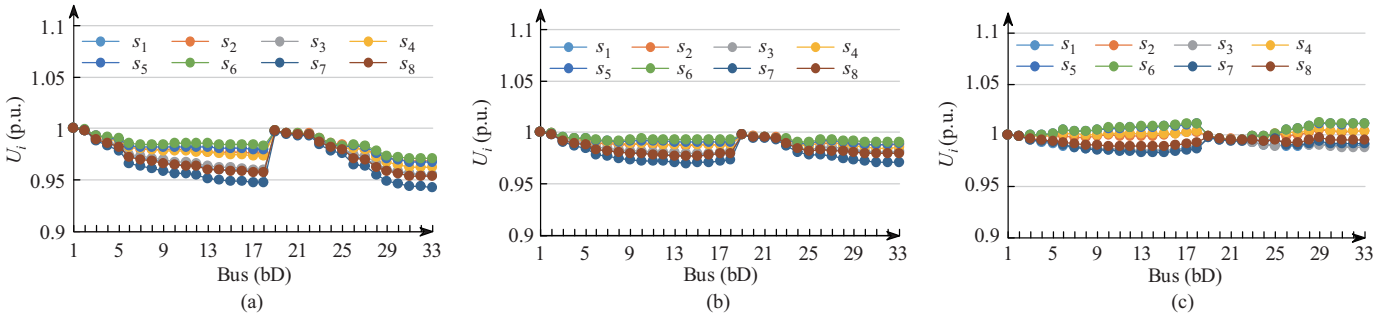

Fig. 11. The bus voltages of DN_4 in different subcases. (a) Results in A1. (b) Results in A2. (c) Results in A3.

5) P2P energy transactions among DNs in A3

P2P energy transactions in A3 is the main focus of this paper, and thus is analyzed in this part. Fig. 12 and Fig. 13(a) show the port powers of U-layer and R-layer at each ER in A3. According to Fig. 13(a), ER_1 and ER_2 purchase or sell electricity in different periods in the P2P market. ER_3 mainly sells electricity, and ER_4 only purchases electricity. The exchanging power of ER_1 will be taken as an example to illustrate detailed energy flow of the ER in the following.

In Fig. 12(a), in s_1 and s_2, power values of the four ports at U-layer in the ER_1 are all negative, which means that energy purchased by ER_1 from R-layer in the P2P market provides energy support to DN_1 through U-layer. Thus, in s_1 and s_2, power of port dC_5 of R-layer in ER_1 shown in Fig. 13(a) is positive, and 1550 kW of electric energy is purchased. According to system structure in Fig. 5(b), port dC_5 of ER_1 is connected to port dC_{13} of ER_2 by $L_{6,14}$. In Table V, ports dC_{13} and dC_{17} at R-layer in ER_2 are interconnected through port dC_{23} at F-layer. Besides, Fig. 13(b) shows that the forwarding power of port dC_{23} is 0 in s_1. Thus, in s_1, the power of 1585 kW from port dC_{13} of ER_2 is transmitted by $L_{6,14}$, and received by port dC_5 of ER_1. Considering energy loss, final power received by ER_1 is 1550 kW. Thus, the configuring capacities of ports dC_5 and dC_{13} are different, and are 1550 and 1600 kVA, respectively.

Similarly, in s_3 and s_6, port powers of U-layer in ER_1 contain positive and negative values, and port powers of U-layer in ER_1 are near zero. Such behaviors mean that ER_1 only aims to regulate the power flow of DN_1 independently in s_3 and s_6.

In s_4 and s_5, ER_1 sells surplus energy of DN_1 in the P2P market through R-layer, and selling powers are 774 and 1139 kW, respectively. Behaviors of ER_1 in s_7 and s_8 are similar to those in s_1 and s_2, and purchasing powers of ER_1 are 1425 and 1432 kW, respectively.

Therefore, simulation results verify that U-layer can regulate power flow of the DN. Surplus energy or demand is sold or met in the P2P market by R-layer.

6) The Energy Forwarding Process of F-layer in A3

Port power at F-layer of ERs is shown in Fig. 13(b). According to Table V, F-layer of ER_2 is configured with two ports dC_{21} (dC_{22}) and dC_{23} (dC_{24}). F-layer of ER_4 is configured with a port dC_{47} (dC_{48}). Take port dC_{21} in ER_2 as an example to illustrate the operation process of the F-layer.

a) Ports of R-layer shared with each other by F-layer.

In Fig. 13(b), in s_1 and s_2, powers of port dC_{21} at F-layer in ER_2 are positive, and are 75 and 150 kW, respectively. While powers of ports dC_{15} and dC_{17} at R-layer is negative. Results indicate that ER_2 sells electric energy in s_1 and s_2. Thus, port dC_{21} at F-layer forwards energy for R-layer.

In Table V, capacities of ports dC_{15} and dC_{17} are 250 and 600 kVA, respectively. In s_1, $P_{18,38,s1}$ is 667 kW. Then port dC_{17} of ER_2 needs to output at least 667 kW, the capacity limit of port dC_{17} will be violated. In such a situation, part of the 667 kW is output from port dC15 and transmitted to $L_{18,38}$ through port dC_{21} of F-layer. In addition, the proposed planning model optimizes loss, and the shared capacity of port dc15 at R-layer will be greater than the excess 67 kW, and is actually 75 kW. Thus, ports of R-layer are shared with each other. The process in s_2 is similar to that in s_1.

b) F-layer forwarding energy for adjacent ERs.

In s_3, power forwarded by port dC_{21} at F-layer is 141 kW, but power of port dC_{15} and dC_{17} at R-layer is zero. Thus, port dC_{21} at F-layer forwards 141 kW of electric energy from ER_3

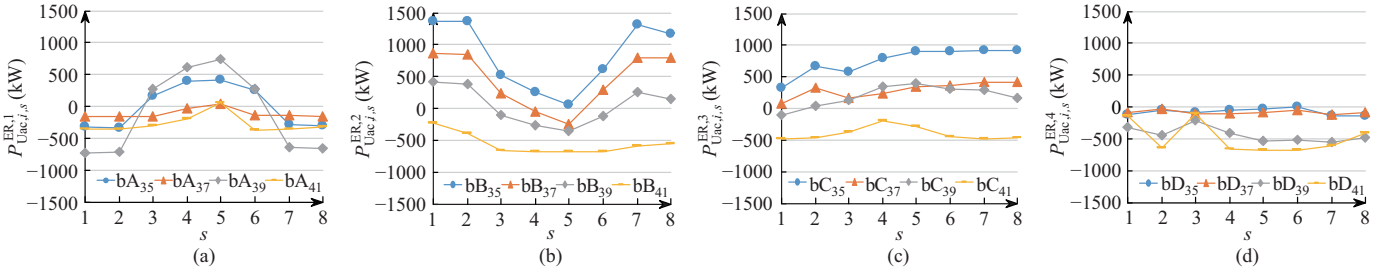

Fig. 12. The active power of U-layer at different ERs in A3. (a) Results of ER_1. (b) Results of ER_2. (c) Results of ER_3. (d) Results of ER_4.

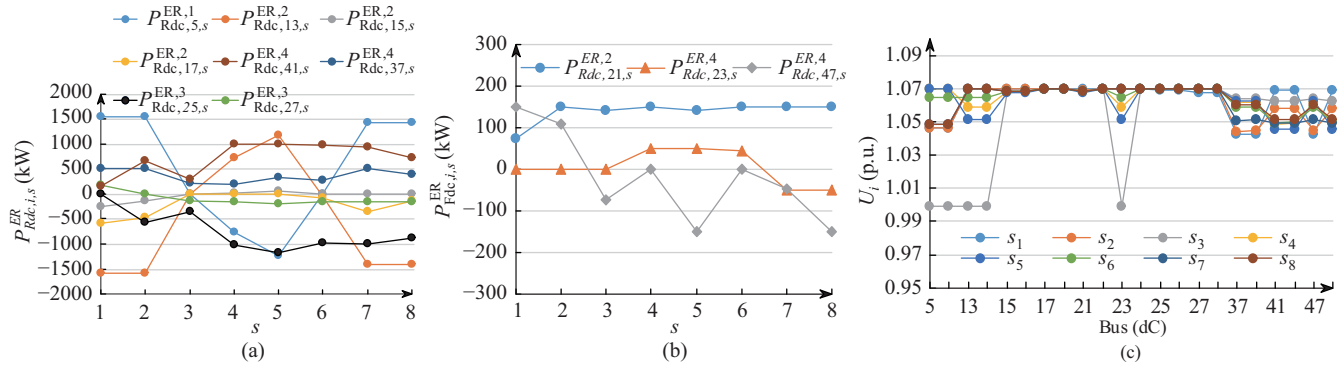

Fig. 13. The power of the R-layer and the F-layer in different ERs, and DC bus voltages in P2P energy sharing network in A3.

to ER_4. For reducing line loss, power of ER_3 is partly output through port dC_{27} at R-layer of ER_3 to ER_2, and forwarded to bus dC_{38} through port dC_{21} at F-layer of ER_2. Combined with the negative power of port dC_{47} in s_3 at F-layer of ER_4 shown in Fig. 13(b), power transmitted by ER_2 finally flows into port dC_{37} at R-layer of ER_4. The operation processes of F-layer is similar in other time slots, and are omitted.

Therefore, simulation results verify that port capacities of R-layer are shared with each other through F-layer, and F-layer can forward energy for adjacent ERs.

7) Voltage analysis of a DC system for P2P energy transactions in A3

Figure 13(c) shows DC voltages of the P2P network. The operating range in this paper is [0.93, 1.07]. According to configuration results of R-layer and F-layer in Table V, DC buses selected to build in A3 are dC_5∼dC_6, dC_{13}∼dC_{18}, dC_{21}∼dC_{28}, dC_{37}∼dC_{38}, dC_{41}∼dC_{42} and dC_{47}∼dC_{48}. Only 22 out of 48 buses are reserved in the scheme. In Fig. 14(c), voltages of the DC system meet the set range.

Therefore, in Case A, simulation results verify the effectiveness of the proposed planning model of ERs considering P2P energy transactions among multiple DNs. The schemes of three layers of ERs can be configured. An ERs-based DNs system can significantly reduce operation cost of each DN, improve power quality of the DNs, reduce exchanging power volatility between the DN and the upstream grid, and promote consumption of DG.

Besides, U-layer can regulate power flow of the DN, and transmit energy from the DN to R-layer, or distribute the energy from R-layer to the DN. R-layer can purchase energy from the P2P market or sell surplus energy. In addition, port capacities of R-layer can be shared with each other through F-layer, and F-layer can also forward energy for the adjacent ERs.

B. Impact of Different Configurations of DG

To verify the generality of the proposed planning model in this paper, three groups of subcases are set to test. 1) B1: configurations of DG are similar to those in Case A, and surplus energy is sufficient; 2) B2: capacities of DG in each DN are insufficient, and no surplus energy exists in each DN in any time slot; 3) B3: the configurations are similar to those in subcase B2, but only a little surplus energy is sold in the P2P market. Configurations of DG are shown in Table VII.

Configuration schemes of each ER in B1, B2, and B3 are shown in Tables VIII, IX and X, respectively. In B1, due to abundant output of DG, sufficient ports in U-layer, R-layer and F-layer of ERs are deployed.

In B2, there is no surplus power to sell in each DN, so

TABLE VII
DIFFERENT CAPACITY CONFIGURATIONS OF DG

Subcase		DN_1	DN_2	DN_3	DN_4
B1	PV	1	5	0	3.5
	WT	1	0	5	4
B2	PV	2.5	2	1.5	2.4
	WT	2	2.5	2.5	1.0
B3	PV	3	2.5	2	3
	WT	2.5	3	3	1.5

TABLE VIII
CAPACITY CONFIGURATIONS OF ERS IN SUBCASE B1

ER_1 (kVA)	ER_2 (kVA)	ER_3 (kVA)	ER_4 (kVA)
Port capacity of U-layer			
bA_{35} (250)	bB_{35} (600)	bC_{35} (1300)	bD_{35} (1100)
bA_{37} (250)	bB_{37} (650)	bC_{37} (950)	bD_{37} (350)
bA_{39} (1000)	bB_{39} (450)	bC_{39} (400)	bD_{39} (1400)
bA_{41} (1050)	bB_{41} (200)	bC_{41} (650)	bD_{41} (500)
Port capacity of R-layer			
dC_1 (600)	dC_{13} (0)	dC_{25} (350)	dC_{37} (100)
dC_3 (1450)	dC_{15} (1300)	dC_{27} (1350)	dC_{39} (1550)
dC_5 (0)	dC_{17} (100)	dC_{29} (450)	dC_{41} (600)
Port capacity of F-layer			
dC_7 (50)	dC_{19} (0)	dC_{31} (0)	dC_{43} (0)
dC_9 (0)	dC_{21} (50)	dC_{33} (0)	dC_{45} (0)
dC_{11} (0)	dC_{23} (50)	dC_{35} (500)	dC_{47} (50)

TABLE IX
CAPACITY CONFIGURATIONS OF ERS IN SUBCASE B2

ER_1 (kVA)	ER_2 (kVA)	ER_3 (kVA)	ER_4 (kVA)
Port capacity of the U-layer			
bA_{35} (400)	bB_{35} (450)	bC_{35} (400)	bD_{35} (250)
bA_{37} (200)	bB_{37} (650)	bC_{37} (450)	bD_{37} (200)
bA_{39} (750)	bB_{39} (200)	bC_{39} (300)	bD_{39} (650)
bA_{41} (550)	bB_{41} (550)	bC_{41} (300)	bD_{41} (400)

TABLE X
CAPACITY CONFIGURATIONS OF ERS IN SUBCASE B3

ER_1 (kVA)	ER_2 (kVA)	ER_3 (kVA)	ER_4 (kVA)
Port capacity of the U-layer			
bA_{35} (500)	bB_{35} (500)	bC_{35} (450)	bD_{35} (0)
bA_{37} (0)	bB_{37} (700)	bC_{37} (600)	bD_{37} (0)
bA_{39} (900)	bB_{39} (0)	bC_{39} (0)	bD_{39} (850)
bA_{41} (750)	bB_{41} (400)	bC_{41} (450)	bD_{41} (300)
Port capacity of R-layer			
dC_1 (0)	dC_{13} (200)	dC_{25} (0)	dC_{37} (0)
dC_3 (0)	dC_{15} (0)	dC_{27} (0)	dC_{39} (0)
dC_5 (200)	dC_{17} (0)	dC_{29} (0)	dC_{41} (0)

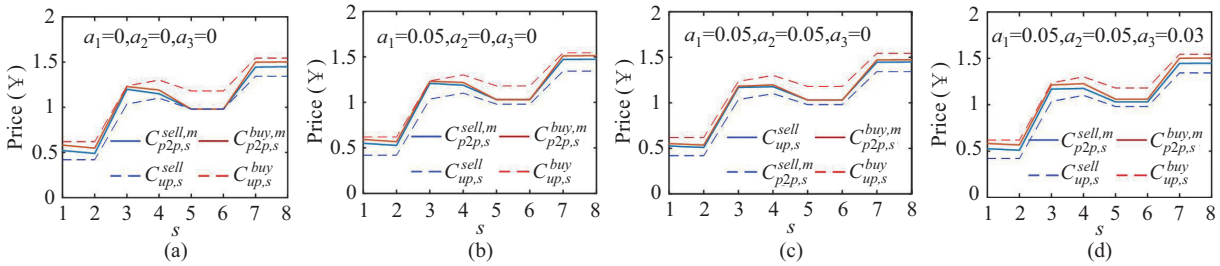

Fig. 14. P2P clearing prices based on the SDR in four subcases. (a) C1. (b) C2. (c) C3. (d) C4.

TABLE XI
EVALUATION INDEXES OF SIMULATION RESULTS IN SUBCASE B1, B2, AND B3

Subcase		f_{sys} (¥)	f_1 (¥)	f_2 (¥)	f_3 (¥)	f_4 (¥)	$\mathrm{K_{var\_1}}$	$\mathrm{K_{var\_2}}$	$\mathrm{K_{var\_3}}$	$\mathrm{K_{var\_4}}$
B1	No ERs	2.894e7	2.080e7	1.451e7	0.021e7	−0.657e7	0.040	3.817	1.601	2.298
	With ERs	2.426e7	2.000e7	1.336e7	−0.109e7	−0.801e7	0.533	1.393	0.114	0.414
B2	No ERs	3.386e7	0.580e7	0.605e7	0.846e7	1.355e7	0.091	0.051	0.101	0.768
	With ERs	3.218e7	0.532e7	0.553e7	0.808e7	1.325e7	0.096	0.051	0.104	0.772
B3	No ERs	1.210e7	0.009e7	0.055e7	0.309e7	0.836e7	0.150	0.078	0.0146	1.239
	With ERs	1.012e7	−0.051e7	−0.007e7	0.263e7	0.806e7	0.127	0.070	0.154	1.248
		$\mathrm{K_{vol\_1}}$	$\mathrm{K_{vol\_2}}$	$\mathrm{K_{vol\_3}}$	$\mathrm{K_{vol\_4}}$	$\mathrm{K_{gap\_1}}$	$\mathrm{K_{gap\_2}}$	$\mathrm{K_{gap\_3}}$	$\mathrm{K_{gap\_4}}$	$\mathrm{K_{gapdc}}$
B1	No ERs	0.028	0.037	0.028	0.034	3.4e-7	3.7e-7	4.0e-7	4.1e-7	–
	With ERs	0.008	0.015	0.012	0.015	9.2e-6	1.0e-5	3.4e-5	9.4e-6	6.7e-5
B2	No ERs	0.009	0.009	0.012	0.023	3.5e-7	3.6e-7	3.5e-7	3.4e-7	–
	With ERs	0.005	0.006	0.007	0.012	8.1e-6	8.3e-6	8.2e-6	7.9e-6	–
B3	No ERs	0.012	0.014	0.012	0.020	1.6e-7	1.7e-7	1.6e-7	1.6e-7	–
	With ERs	0.010	0.012	0.010	0.015	6.4e-6	4.1e-6	3.9e-6	3.7e-6	5.5e-7

each router is only configured with ports at U-layer. Thus, P2P energy sharing among DNs does not exist.

In B3, only DN_1, DN_2 and DN_4 have maximum power of 700 kW in some time slots. Investing costs of R-layer and electric lines are high, and only R-layers of ER_1 and ER_2 are configured with only one port. Thus, P2P energy sharing only exists between DN_1 and DN_2.

Corresponding indexes of the three subcases are shown in Table XI. For each subcase, simulation of each DN without any ER is implemented, and simulations of DNs with ERs by deploying the proposed planning of ERs are also carried out. Obviously, configuring the ER can improve operation of the DN in terms of operation cost, bus voltage. Power volatility between the DN and the upstream grid is reduced in B1 as a whole.

Therefore, in subcases A3, B1, B2, and B3, simulation results verify the proposed planning model of ERs in this paper can be applied to different configurations of DG. Thus, the proposed planning model is general.

C. Impact of Different Price Mechanisms

P2P clearing price is based on the fixed gap based mechanism in Case A and B, as shown in Fig. 6(d). This section will explore the impact of the SDR-based clearing price mechanism on configuration of ERs. The configurations of DG are the same as those in Case A3.

Values of NP_s in (49) are roughly estimated based on powers shown in Fig. 7(a). Four subcases are set. 1) C1: $a_1 = 0$, $a_2 = 0$, and $a_3 = 0$. Protections of the lowest selling price, highest selling price and price difference of the P2P market are not considered in C1. 2) C2: $\mathrm{a}_1 = 0.05$, $a_2 = 0$, and $a_3 = 0$. Protections of the lowest selling price are considered in C2. 3) C3: $a_1 = 0.05$, $a_2 = 0.05$, and $a_3 = 0$. Protections of the lowest selling price and highest selling price are considered in C3. 4) C4: $a_1 = 0.05$, $a_2 = 0.05$, and $a_3 = 0.03$. Protections of the lowest selling price, highest selling price and price difference of the P2P market are considered in C4. P2P prices of four subcases are shown in Fig. 14(a)–(d), respectively. Optimization results are shown in Table XII.

Results in Table XII show that: 1) under both P2P price mechanisms, each participant can reduce comprehensive cost or increase income; 2) compared with the fixed gap based mechanism, the SDR based mechanism reduces more of the total cost of the entire system; 3) DNs with more surplus energy tend to benefit more in both mechanisms.

TABLE XII
SIMULATION RESULTS WITH DIFFERENT P2P CLEARING PRICES

Subcase	f_{sys} (¥)	f_1 (¥)	f_2 (¥)	f_3 (¥)	f_4 (¥)
A1	2.122e7	1.186e7	−0.222e7	−0.770e7	1.927e7
A3	1.597e7	1.068e7	−0.400e7	−0.913e7	1.843e7
C1	1.565e7	1.092e7	−0.447e7	−0.893e7	1.813e7
C2	1.537e7	1.093e7	−0.464e7	−0.929e7	1.836e7
C3	1.530e7	1.075e7	−0.443e7	−0.916e7	1.813e7
C4	1.575e7	1.088e7	−0.434e7	−0.922e7	1.844e7

Therefore, simulation results verify the proposed planning model of ERs considering P2P energy sharing among DNs are effective under different P2P clearing prices.

D. Impact of Different Solvers on the Configuration Scheme

Since the proposed planning model is complex, different solvers are implemented to solve subcase A3 to analyze derived configuration schemes. Under conventional solvers XPRESS, GUROBI, CPLEX, and MOSEK, configuration cost of each DN is shown in Table XIII. Subcase A1 can be employed to explain clearly, that configuration of the energy router can benefit participating distribution networks. Detailed implementation of subcase A1 which no ER is considered in DN and can be found in Case A.

TABLE XIII
SIMULATION RESULTS WITH DIFFERENT P2P CLEARING PRICES

Subcase	f_{sys} (¥)	f_1 (¥)	f_2 (¥)	f_3 (¥)	f_4 (¥)
A1	2.122e7	1.186e7	−0.222e7	−0.770e7	1.927e7
XPRESS	1.597e7	1.068e7	−0.400e7	−0.913e7	1.843e7
GUROBI	1.593e7	1.065e7	−0.406e7	−0.915e7	1.849e7
CPLEX	1.593e7	1.069e7	−0.405e7	−0.915e7	1.844e7
MOSEK	–	–	–	–	–

In Table XIII, except the MOSEK solver fails to derive a scheme of ERs, configuration costs of the rest of the solvers are similar, but different. It is reasonable because different solvers have different algorithms. Besides, considering the planning model is complex in the case study, that a solver can't solve some problems is normal, such as MOSEK in this paper. Among them, XPRESS can solve more scenarios of the proposed model in this paper through many tests, and thus is adopted in Case A∼Case C. Besides, the derived schemes

of ERs under different solvers are different, which means the proposed planning model has more than one scheme of ERs under the same configuration of DNs and DG. But all the schemes are effective. As for which scheme is the best, it is limited to space and omitted in this paper.

Therefore, simulation results show the proposed planning model has more solutions on the scheme of ERs under similar system costs. More effective solvers are expected to the proposed planning model in this paper.

E. Discussions

1) The interest of each participant

In this paper, the planning model of the energy router is the main focus. Considering the peer-to-peer trading model in [32] is solved in a centralized way, the proposed model is also solved in the same way.

However, if the model is solved in a typical centralized way only, it is unclear whether each participant's interest can be ensured in most scenarios. In [38], peer-to-peer trading is solved in a centralized way, but each participant can benefit from peer-to-peer trading. In [36], peer-to-peer trading is solved in a distributed way, but the model is essentially a centralized one.

Considering that benefits of some participants may be impaired to achieve a better solution as a whole, the benefit of each participant is allocated according to their contributions in [38]. Thus, some additional constraints can be added to improve the situation mentioned above if the model is solved in a typical centralized way.

In this paper, only a distribution system with energy surplus can sell energy to other distribution systems, and only a distribution system with energy shortage can purchase energy from other distribution systems. Such behaviors are guaranteed by constraints (44) and (45). Besides, the selling price (purchasing price) in the peer-to-peer trading market is higher (lower) than in the upstream grid. Thus, it is reasonable that selling or purchasing energy through peer-to-peer trading can benefit all participants. Then, the interest of each participant can be ensured.

In the case study, results show that all participants can gain benefits. Especially in Case B, results of subcases B1, B2, and B3 show that only when the configuration of the energy router can benefit a distribution system itself will the energy router be deployed in that system. Besides, the distribution network with more surplus energy to sell gains the most benefit, which is reasonable.

Thus, we think the interest of each energy router-based distribution network can be ensured in this paper.

If a participant cannot gain benefits in a particular application, capacity configuration of R-layer in an ER should be reduced until that participant can gain benefits. The detailed process is omitted in this paper. After all, if there is no peer-to-peer energy trading, configurations of ERs will be independent of each other.

2) Computation efficiency and optimality of the proposed model

In this paper, the proposed planning model considering energy router-based distribution networks is the main focus, and the model is solved by solvers in commercial software GAMS. Since the primary proposed model is nonlinear in power flow calculation, it is difficult to derive a good solution.

For achieving a better solution, the proposed model is converted into a MISOCP-based planning model to solve efficiently. Such a process has been deployed in many studies such as [29]. Discussion of the computation efficiency and optimality of the proposed model belongs to that of the general MISOCP-based algorithm itself. Because complex constraints may divide the second-order cone, even the MISOCP-based model may derive local rather than global optimal solutions [39]. It is essentially a critical and challenging problem for the MISOCP-based algorithm itself, which will not be omitted in this paper.

In subcase D of Section IV, four kinds of solvers in GAMS are deployed to validate the proposed model. Differences in results are very tiny, which verify that optimal results are derived.

V. Conclusion

With a high proportion of DG in the DN, the DN is faced with issues such as power quality caused by surplus energy and surplus electricity sold to the upstream grid at a low price. In this paper, a planning model of ERs considering P2P energy transactions among DNs is established. Economical operation of ERs-based DNs under P2P transactions is preliminarily explored. Conclusions are as follows.

1) ERs-based DNs with P2P energy transactions can effectively reduce comprehensive operation cost of each DN, or improve revenue. Among them, under different P2P price mechanisms, the electric energy seller benefits the most in the P2P market.

2) Configuration of the ER reduces voltage deviation of the DN, promotes consumption of DG, and significantly improves voltage quality of the DN. With P2P energy sharing, cooperative consumption of power fluctuations within DNs are achieved at the same rated voltage side. Thus, the impact from the DN on the upstream grid is alleviated.

3) When the ER implements P2P energy sharing, U-layer can transmit surplus energy of the DN to R-layer, or distribute the energy purchased by R-layer to each port of U-layer. Without P2P energy sharing, R-layer is in standby mode, and U-layer optimizes power flow of the DN. Based on dispatching results, port capacities of R-layer can share with each other by F-layer, or F-layer forwards power of adjacent ERs;

There is little research on ER planning in a DN from the perspective of power flow optimization. Preliminary exploration on analysis of economical operation in ERs-based DNs is conducted in this paper. A P2P energy trading mechanism and scheduling model of F-layer need to be further explored in future work.

Appendix

A. The Detailed MISOCP-based Planning Model

The detailed MISOCP-based planning model is shown from (A1)–(A2). The decision variables are $\pi_{\mathrm{Uac},j}^{\mathrm{ER},m}$, $\pi_{\mathrm{Rdc},j}^{\mathrm{ER},m}$, $\pi_{\mathrm{Fdc},j}^{\mathrm{ER},m}$,

$\delta^{\mathrm{ER},m}_{\mathrm{Uac},j}$ and $\delta^{\mathrm{ER},m}_{\mathrm{Rdc},j}$.

$$\min f_{\mathrm{sys}} = \sum_{m=1}^{N^{\mathrm{DN}}} f_m\left(\pi^{\mathrm{ER},m}_{\mathrm{Uac},j}, \pi^{\mathrm{ER},m}_{\mathrm{Rdc},j}, \pi^{\mathrm{ER},m}_{\mathrm{Fdc},j}, \delta^{\mathrm{ER},m}_{\mathrm{Uac},j}, \delta^{\mathrm{ER},m}_{\mathrm{Rdc},j}\right) \tag{A1}$$

s.t. (77)–(79) (A2)

$$\sum_{j:j\to k}(P_{jk,s} - r^{\mathrm{er},m}_{jk}\hat{I}_{jk,s}) = P^{\mathrm{ER},m}_{\mathrm{Uac},k,s},$$
$$j \in N^{\mathrm{ER},m}_{\mathrm{Ulac}},\ k \in N^{\mathrm{ER},m}_{\mathrm{Uac}}$$
$$\sum_{j:j\to k}(Q_{jk,s} - x^{\mathrm{er},m}_{jk}\hat{I}_{jk,s}) = Q^{\mathrm{ER},m}_{\mathrm{Uac},k,s},$$
$$j \in N^{\mathrm{ER},m}_{\mathrm{Ulac}},\ k \in N^{\mathrm{ER},m}_{\mathrm{Uac}}$$
$$\hat{U}_{i,s}\hat{I}_{ij,s} \geq P^2_{ij,s} + Q^2_{ij,s},\ i\to j,\ i \in N^{\mathrm{ER},m}_{\mathrm{Ulac}},\ j \in N^{\mathrm{ER},m}_{\mathrm{Uac}}$$
$$\hat{U}_{j,s} = \hat{U}_{i,s} - 2(r^{\mathrm{er},m}_{ij}P_{ij,s} + x^{\mathrm{er},m}_{ij}Q_{ij,s}) +$$
$$\hat{I}_{ij,s}[(r^{\mathrm{er},m}_{ij})^2 + (x^{\mathrm{er},m}_{ij})^2],\ i\to j,\ i \in N^{\mathrm{ER},m}_{\mathrm{Ulac}},\ j \in N^{\mathrm{ER},m}_{\mathrm{Uac}}$$
$$(P^{\mathrm{ER},m}_{\mathrm{Uac},i,s})^2 + (Q^{\mathrm{ER},m}_{\mathrm{Uac},i,s})^2 \leq (S^{\mathrm{ER},m}_{\mathrm{Uac},i})^2,\ i \in N^{\mathrm{ER},m}_{\mathrm{Uac}}$$
$$\sum_{i:i\to j}(P_{ij,s} - r^{\mathrm{L},m}_{ij}\hat{I}_{ij,s}) = \sum_{j:j\to k}P_{jk,s},$$
$$j \in N^{\mathrm{ER},m}_{\mathrm{Ulac}},\ k \in N^{\mathrm{ER},m}_{\mathrm{Uac}}$$
$$\sum_{i:i\to j}(Q_{ij,s} - x^{\mathrm{L},m}_{ij}\hat{I}_{ij,s}) = \sum_{j:j\to k}Q_{jk,s},$$
$$j \in N^{\mathrm{ER},m}_{\mathrm{Ulac}},\ k \in N^{\mathrm{ER},m}_{\mathrm{Uac}}$$
$$\hat{U}_{i,s}\hat{I}_{ij,s} \geq P^2_{ij,s} + Q^2_{ij,s},\ i\to j,\ i \in N^{\mathrm{bus},m}_{\mathrm{ac}},\ j \in N^{\mathrm{ER},m}_{\mathrm{Ulac}}$$
$$\hat{U}_{j,s} = \hat{U}_{i,s} - 2(r^{\mathrm{L},m}_{ij}P_{ij,s} + x^{\mathrm{L},m}_{ij}Q_{ij,s}) +$$
$$\hat{I}_{ij,s}[(r^{\mathrm{L},m}_{ij})^2 + (x^{\mathrm{L},m}_{ij})^2],\ i\to j,\ i \in N^{\mathrm{bus},m}_{\mathrm{ac}},\ j \in N^{\mathrm{ER},m}_{\mathrm{Ulac}}$$
$$(P_{ij,s})^2 + (Q_{ij,s})^2 \leq (S^{\mathrm{N}}_{ij})^2,\ i \in N^{\mathrm{bus},m}_{\mathrm{ac}},\ j \in N^{\mathrm{ER},m}_{\mathrm{Ulac}}$$
(12)–(23)

$$P^m_{\mathrm{netloss}} = \sum_{s,i\to j} r_{ij}\hat{I}_{ij,s},\ i,j \in N^{\mathrm{bus},m}_{\mathrm{ac}}$$
$$P^m_{\mathrm{acloss}} = \sum_{s,i\to j} r^{\mathrm{L}}_{ij}\hat{I}_{ij,s},\ i \in N^{\mathrm{bus},m}_{\mathrm{ac}},\ j \in N^{\mathrm{ER},m}_{\mathrm{Ulac}} \tag{A3}$$
$$P^m_{\mathrm{dcloss}} = \begin{cases} \frac{1}{2}\sum_{s,\ i\in N^{\mathrm{ER},m}_{\mathrm{ldc}}} r_{ij}\hat{I}_{ij,s}, & \text{if } i\to j \\ \frac{1}{2}\sum_{s,\ i\in N^{\mathrm{ER},m}_{\mathrm{ldc}}} r_{ij}\hat{I}_{ji,s}, & \text{else} \end{cases}$$
$$P^{\mathrm{ER},m}_{\mathrm{Uloss}} = \sum_{s,i\to j} r^{\mathrm{er}}_{jk}\hat{I}_{ij,s},\ i \in N^{\mathrm{ER},m}_{\mathrm{Ulac}},\ j \in N^{\mathrm{ER},m}_{\mathrm{Uac}}$$
$$P^{\mathrm{ER},m}_{\mathrm{Rloss}} = \begin{cases} \sum_{s,i\to j} r_{ij}\hat{I}_{ij,s}, & \text{if } i \in N^{\mathrm{ER},m}_{\mathrm{Rdc}} \\ \sum_{s,i\to j} r_{ij}\hat{I}_{ij,s}, & \text{if } j \in N^{\mathrm{ER},m}_{\mathrm{Rdc}} \end{cases}$$
$$P^{\mathrm{ER},m}_{\mathrm{Rloss}} = \begin{cases} \sum_{s,i\to j} r_{ij}\hat{I}_{ij,s}, & \text{if } i \in N^{\mathrm{ER},m}_{\mathrm{Rdc}} \\ \sum_{s,i\to j} r_{ij}\hat{I}_{ij,s}, & \text{if } j \in N^{\mathrm{ER},m}_{\mathrm{Rdc}} \end{cases} \tag{A4}$$
$$P^{\mathrm{ER},m}_{\mathrm{Floss}} = \sum_{s,i\to j} r_{ij}\hat{I}_{ij,s},\ i \in N^{\mathrm{ER},m}_{\mathrm{Rldc}},\ j \in N^{\mathrm{ER},m}_{\mathrm{Fdc}}$$
(30)–(37) and (40)–(41) and (44)–(45)

$$\sum_{i:i\to k}\hat{I}_{\mathrm{ik,s}} \leq M_1\delta^{\mathrm{ER},m}_{\mathrm{Uac},l},\ i \in N^{\mathrm{bus}}_{\mathrm{ac}},\ k \in N^{\mathrm{ER},m}_{\mathrm{Ulac}}$$
$$\sum_{i:i\to j}\hat{I}_{ij,s} \leq M_2\pi^{\mathrm{ER},m}_{\mathrm{Uac},j},\ i \in N^{\mathrm{ER},m}_{\mathrm{Ulac}},\ j \in N^{\mathrm{ER},m}_{\mathrm{Uac}}$$
$$\begin{cases} \sum_{i\to j}\hat{I}_{ij,s} \leq M_1\delta^{\mathrm{ER},m}_{\mathrm{Rdc},i}, & \text{if } i \in N^{\mathrm{ER},m}_{\mathrm{Rldc}} \\ \sum_{i\to j}\hat{I}_{ij,s} \leq M_1\delta^{\mathrm{ER},m}_{\mathrm{Rdc},j}, & \text{if } j \in N^{\mathrm{ER},m}_{\mathrm{Rldc}} \end{cases}$$
$$\begin{cases} \sum_{i\to j}\hat{I}_{ij,s} \leq M_2\pi^{\mathrm{ER},m}_{\mathrm{Rdc},i}, & \text{if } i \in N^{\mathrm{ER},m}_{\mathrm{Rdc}} \\ \sum_{i\to j}\hat{I}_{ij,s} \leq M_2\pi^{\mathrm{ER},m}_{\mathrm{Rdc},j}, & \text{if } j \in N^{\mathrm{ER},m}_{\mathrm{Rdc}} \end{cases}$$
$$\sum_{i:i\to j}\hat{I}_{ij,s} \leq M_5\pi^{\mathrm{ER},m}_{\mathrm{Fdc},j,s},\ i \in N^{\mathrm{ER},m}_{\mathrm{Fldc}},\ j \in N^{\mathrm{ER},m}_{\mathrm{Fdc}}$$
$$\sum_{i:i\to j}(P_{ij,s} - r_{ij}\hat{I}_{ij,s}) + P_{gj,s}$$
$$= \sum_{j\in N^{\mathrm{ER},m}_{\mathrm{Rdc}}} P^{\mathrm{ER},m}_{\mathrm{Rdc},j,s} + \sum_{j\in N^{\mathrm{ER},m}_{\mathrm{Fdc}}} P^{\mathrm{ER},m}_{\mathrm{Fdc},j,s}$$
$$+ P_{dj,s} + \sum_{k:j\to k} P_{jk,s},\ i,j,k \in N^{\mathrm{bus}}_{\mathrm{dc}}$$
$$\hat{U}_{j,s} = \hat{U}_{i,s} - 2r_{ij}P_{ij,s} + \hat{I}_{ij,s}r^2_{ij},\ i\to j,\ i,j \in N^{\mathrm{bus}}_{\mathrm{dc}}$$
$$\hat{U}_{i,s}\hat{I}_{ij,s} \geq P^2_{ij,s},\ i\to j,\ i,j \in N^{\mathrm{bus}}_{\mathrm{dc}}$$
(56)–(58) and (63)–(65)

$$\sum_{i:i\to j}(P_{ij,s} - r_{ij}\hat{I}_{ij,s}) + P_{gj,s} = P_{dj,s} + \sum_{k:j\to k} P_{jk,s},$$
$$i,\ j \in N^{\mathrm{bus},m}_{\mathrm{ac}}$$
$$\sum_{i:i\to j}(Q_{ij,s} - x_{ij}\hat{I}_{ij,s}) + Q_{gj,s} = Q_{dj,s} + \sum_{k:j\to k} Q_{jk,s},$$
$$i,\ j \in N^{\mathrm{bus},m}_{\mathrm{ac}}$$
$$\hat{U}_{j,s} = \hat{U}_{i,s} - 2(r_{ij}P_{ij,s} + x_{ij}Q_{ij,s}) + \hat{I}_{ij,s}z^2_{ij},$$
$$i\to j,\ i,j \in N^{\mathrm{bus},m}_{\mathrm{ac}}$$
$$\hat{U}_{i,s}\hat{I}_{ij,s} \geq P^2_{ij,s} + Q^2_{ij,s},\ i\to j,\ i,j \in N^{\mathrm{bus},m}_{\mathrm{ac}} \tag{A5}$$

REFERENCES

[1] P. Y. Wang, F. Y. Liang, J. Y. Song, N. Q. Jiang, X. P. Zhang, L. Guo, and X. X. Gu, "Impact of the PV Location in Distribution Networks on Network Power Losses and Voltage Fluctuations with PSO Analysis," *CSEE Journal of Power and Energy Systems*, vol. 8, no. 2, pp. 523–534, Mar. 2022.

[2] A. Ali, M. U. Keerio, and J. A. Laghari, "Optimal site and size of distributed generation allocation in radial distribution network using multi-objective optimization," *Journal of Modern Power Systems and Clean Energy*, vol. 9, no. 2, pp. 404–415, Mar. 2021.

[3] Z. H. Huang, Y. C. Zhang, F. Zheng, J. H. Lin, X. L. An, and H. Shi, "Day-ahead and real-time energy management for active distribution network based on coordinated optimization of different stakeholders," *Power System Technology*, vol. 45, no. 6, pp. 2299–2307, Jun. 2021.

[4] E. B. Luo, P. W. Cong, H. Lu, and Y. H. Li, "Two-stage hierarchical congestion management method for active distribution networks with multi-type distributed energy resources," *IEEE Access*, vol. 8, pp. 120309–120320, Jun. 2020.

[5] Y. H. Yang, W. Pei, Q. H. Huo, J. J. Sun, and F. Xu, "Coordinated planning method of multiple micro-grids and distribution network with flexible interconnection," *Applied Energy*, vol. 228, pp. 2361–2374, Oct. 2018,

[6] M. Fu, Z. Y. Xu, N. Wang, X. Lyu, and W. S. Xu, "Peer-to-peer plus" electricity transaction within community of active energy agents regarding distribution network constraints," *Energies*, vol. 13, no. 9, pp. 2408, May 2020.

[7] H. Guo, F. Wang, L. Li, L. J. Zhang, and J. Luo, "A minimum loss routing algorithm based on real-time transaction in energy Internet," *IEEE Transactions on Industrial Informatics*, vol. 15, no. 12, pp. 6446–6456, Dec. 2019.

[8] K. Alzaareer, M. Saad, H. Mehrjerdi, D. Asber, and S. Lefebvre, "Development of new identification method for global group of controls for online coordinated voltage control in active distribution networks," *IEEE Transactions on Smart Grid*, vol. 11, no. 5, pp. 3921–3931, Sep. 2020.

[9] S. Maharjan, A. M. Khambadkone, and J. C. H. Peng, "Robust constrained model predictive voltage control in active distribution networks," *IEEE Transactions on Sustainable Energy*, vol. 12, no. 1, pp. 400–411, Jan. 2021.
[10] A. Q. Huang, M. L. Crow, G. T. Heydt, J. P. Zheng, and S. J. Dale, "The future renewable electric energy delivery and management (FREEDM) system: The energy Internet," *Proceedings of the IEEE*, vol. 99, no. 1, pp. 133–148, Jan. 2011.
[11] Y. Xu, J. H. Zhang, W. Y. Wang, A. Juneja, and S. Bhattacharya, "Energy router: architectures and functionalities toward energy Internet," in *Proceedings of 2011 IEEE International Conference on Smart Grid Communications (SmartGridComm)*, 2011.
[12] M. A. Shamshuddin, F. Rojas, R. Cardenas, J. Pereda, M. Diaz, and R. Kennel, "Solid state transformers: concepts, classification, and control," *Energies*, vol. 13, no. 9, pp. 2319, May 2020.
[13] Y. S. Liu, Y. Fang, and J. Li, "Interconnecting microgrids via the energy router with smart energy management," *Energies*, vol. 10, no. 9, 1297, Sep. 2017.
[14] C. M. Tu, F. Xiao, Z. Lan, Q. Guo, and Z. K. Shuai, "Analysis and control of a novel modular-based energy router for DC microgrid cluster," *IEEE Journal of Emerging and Selected Topics in Power Electronics*, vol. 7, no. 1, pp. 331–342, Mar. 2019.
[15] H. C. Shi, H. Q. Wen, Y. H. Hu, Y. Yang, and Y. W. Wang, "Efficiency optimization of dc solid-state transformer for photovoltaic power systems," *IEEE Transactions on Industrial Electronics*, vol. 67, no. 5, pp. 3583–3595, May 2020.
[16] M. F. Chen, M. C. Xia, and Q. F. Chen, "Research on distributed source-load interaction strategy considering energy router based active distribution network," *IEEE Access*, vol. 7, pp. 150505–150516, Oct. 2019.
[17] Y. L. Xu, H. B. Sun, and W. Gu, "A novel discounted min-consensus algorithm for optimal electrical power trading in grid-connected DC microgrids," *IEEE Transactions on Industrial Electronics*, vol. 66, no. 11, pp. 8474–8484, Nov. 2019.
[18] X. Y. Shi, Y. L. Xu, and H. B. Sun, "A biased min-consensus-based approach for optimal power transaction in multi-energy-router systems," *IEEE Transactions on Sustainable Energy*, vol. 11, no. 1, pp. 217–218, Jan. 2020.
[19] J. Q. Miao, N. Zhang, C. Q. Kang, J. X. Wang, Y. Wang, and Q. Xia, "Steady-state power flow model of energy router embedded AC network and its application in optimizing power system operation," *IEEE Transactions on Smart Grid*, vol. 9, no. 5, pp. 4828–4837, Sep. 2018.
[20] J. Guo, K. J. Li, J. S. Wang, and K. Q. Sun, "Power flow calculation model and feasible solution of AC-DC network with energy routers," *Automation of Electric Power Systems*, vol. 42, no. 13, pp. 85–93, Jul. 2018.
[21] J. Q. Miao, N. Zhang, and C. Q. Kang, "Analysis on the influence of energy router on the optimal operation of distribution network," *Proceedings of the CSEE*, vol. 37, no. 10, pp. 2832–2839, May 2017.
[22] T. Wu, C. H. Zhao, and Y. J. A. Zhang, "Distributed AC-DC optimal power dispatch of VSC-based energy routers in smart microgrids," *IEEE Transactions on Power Systems*, vol. 36, no. 5, pp. 4457–4470, Sep. 2021.
[23] L. Huang, C. X. Zong, X. Yang, W. J. Chen, Y. X. Zhu, and K. T. Bi, "Power flow calculation of distribution network with multiple energy routers," *IEEE Access*, vol. 9, pp. 23489–23497, Dec. 2021.
[24] Q. Geng, Y. Hu, J. Z. He, Y. Y. Zhou, W. Zhao, X. X. Xu, and W. Wei, "Optimal operation of AC-DC distribution network with multi park integrated energy subnetworks considering flexibility," *IET Renewable Power Generation*, vol. 14, no. 6, pp. 1004–1019, Apr. 2020.
[25] Q. Geng, Y. Hu, J. Z. He, Y. Y. Zhou, and W. Zhao, "Optimal power flow for hybrid ac/dc grid with power electronic transformer," *Power System Technology*, vol. 43, no. 9, pp. 3288–3296, Sep. 2019.
[26] L. Dong, T. Zhang, T. J. Pu, .N. S. Chen, and Y. Y. Sun, "A decentralized optimal operation of AC/DC hybrid microgrids equipped with power electronic transformer," *IEEE Access*, vol. 7, pp. 157946–157959, Oct. 2019.
[27] I. Syed, V. Khadkikar, and H. H. Zeineldin. "Loss reduction in radial distribution networks using a solid-state transformer," *IEEE Transactions on Industry Applications*, vol. 54, no. 5, pp. 5474–5482, Sep./Oct. 2018.
[28] L. Huang, Y. X. Li, Q. Cui, N. Xie, J. Zeng, and J. Shu, "Research on optimal configuration of AC/DC hybrid system integrated with multiport solid-state transforms and renewable energy based on a coordinate strategy," *International Journal of Electrical Power & Energy Systems*, vol. 119, pp. 105880, Jul. 2020.
[29] C. S. Wang, G. Y. Song, P. Li, H. R. Ji, J. L. Zhao, and J. Z. Wu, "Optimal siting and sizing of soft open points in active electrical distribution networks," *Applied Energy*, vol. 189, pp. 301–309, Mar. 2017.
[30] J. L. Zhao, H. Chen, G. Y. Song, X. M. Fan, P. Li, and J. Z. Wu, "Planning method of soft open point in distribution network considering reliability benefits," *Automation of Electric Power Systems*, vol. 44, no. 10, pp. 22–31, May 2020.
[31] M. F. Chen, M. C. Xia, and Q. F. Chen, "Hierarchical structure design and primary energy dispatching strategy of net energy router," *Electric Power Systems Research*, vol. 201, pp. 107539, Dec. 2021.
[32] D. L. Rodrigues, X. M. Ye, X. H. Xia, and B. Zhu, "Battery energy storage sizing optimisation for different ownership structures in a peer-to-peer energy sharing community," *Applied Energy*, vol. 262, pp. 114498, Mar. 2020.
[33] N. Liu, X. H. Yu, C. Wang, C. J. Li, L. Ma, and J. Y. Lei. "Energy-sharing model with price-based demand response for microgrids of peer-to-peer prosumers," *IEEE Transactions on Power Systems*, vol. 32, no. 5, pp. 3569–3583, Sep. 2017.
[34] X. L. Liu, Y. B. Liu, H. Yin, J. Y. Liu, and X. D. Yuan, "Network planning of AC/DC hybrid distribution system with power electronic transformers," *High Voltage Engineering*, vol. 47, no. 4, pp. 1283–1294, Apr. 2021.
[35] Y. Y. Chen, G. C. Geng, Q. Y. Jiang, J. H. Li, Z. Q. Zhou, and C. L. Wang, "Optimal siting and sizing method of soft open point in distribution network combined with traditional regulations," *High Voltage Engineering*, vol. 46, no. 4, pp. 1181–1188, Apr. 2020.
[36] X. Y. He, P. Dong, M. B. Liu, X. W. Huang, W. L. Deng, and R. J. He, "P2P energy trading considering prosumer preference and system risk," *CSEE Journal of Power and Energy Systems*. DOI: 10.17775/CSEE-JPES.2021.06870.
[37] W. X. Liu, M. D. Fu, M. Y. Yang, Y. H. Yang, L. F. Wang, R. J. Wang, and T. Y. Zhao, "A Bi-level interval robust optimization model for service restoration in flexible distribution networks," *IEEE Transactions on Power Systems*, vol. 36, no. 3, pp. 1843–1855, May 2021.
[38] Y. Hu, C. C. Zhou, X. Y. Ma, Z. Y. Yuan, J. Y. Lei, B. Tian, J. J. Shan, and J. J. Hu, "Establishment and simulation of prosumers transaction model in P2P mode," *Electric Power*, vol. 52, no. 11, pp. 44–50, Nov. 2019.
[39] L. G. Gan, N. Li, U. Topcu, and S. H. Low, "Exact convex relaxation of optimal power flow in radial networks," *IEEE Transactions on Automatic Control*, vol. 60, no. 1, pp. 72–87, Jan. 2015.

Meifu Chen received a B.S. degree in Electrical Engineering and Automatization specialty from Beijing Forestry University, Beijing, China, in 2014, and an M.S. degree in Electrical Engineering from Beijing Jiaotong University, Beijing, China, in 2017. He is currently pursuing a Ph.D. degree in Electrical Engineering with Beijing Jiaotong University, Beijing, China. His research interests include optimal operations of active distribution networks based on energy routing, and energy routers.

Mingchao Xia received B.S. and Ph.D. degrees in Electrical Engineering from Tsinghua University, Beijing, China, in 1998 and in 2003, respectively. He is currently a Professor with the School of Electrical Engineering, Beijing Jiaotong University. His current research interests include intelligent power distribution system control and optimization, power electronics in power distribution, and flexible load control.

Qifang Chen received B.S. and M.S. degrees from Xiangtan University, Hunan, China, in 2010 and 2013, respectively, in Communication Engineering and Electric Engineering, and a Ph.D. degree in Electrical and Electronic Engineering, North China Electric Power University, Beijing, China, in 2017. He is currently an Associate Professor with the School of Electrical Engineering Beijing Jiaotong University. His research interests include demand side energy management, and the electric vehicle charging station.